PERGAMON

International Journal of Solids and Structures 38 (2001) 547–576

INTERNATIONAL JOURNAL OF SOLIDS and STRUCTURES

www.elsevier.com/locate/ijsolstr

Rate-dependent interface models: formulation and numerical applications

Alberto Corigliano *, Michele Ricci

Department of Structural Engineering, Politecnico di Milano, Piazza Leonardo da Vinci 32, 20133 Milano, Italy

Received 3 March 1999; in revised form 8 March 2000

Abstract

In this paper, two rate-dependent interface models are formulated and discussed. The models are conceived for the simulation of debonding degradation in polymer matrix composites, the most meaningful example of application being the simulation of rate-dependent delamination. Numerical time integration and the introduction in a finite element analysis program are described in detail; numerical examples and a comparison with experimental results are presented.

Keywords: Interface models; Composite delamination; Rate dependency

1. Introduction

Interface degradation represents a major damage phenomenon in various situations, among them debonding and delamination in composites (Garg, 1988), fracture in rock joints and masonry (Satmani Naresh et al., 1996), decohesion of films from substrates (Jensen et al., 1990).

In order to simulate interface degradation, and more generally complex fracture propagation processes (see e.g. Pandolfi et al. (1999) for a recent application), it is made increasingly use in the literature of interface models relating tractions to displacement discontinuities along a surface of potential decohesion.

The subject of the present paper is the development of interface models for the simulation of time-dependent delamination. It is widely recognised (Bradley, 1989) that the major contribution to delamination fracture resistance is given by the damage developing in the matrix-rich interlaminar layer. This fact justifies the application of interface models to the study of delamination (Allix and Ladeveze, 1992; Corigliano, 1993; Schellekens and De Borst, 1993; Crisfield et al., 1997). By assuming the dissipative processes during fracture to be localised at the interface between laminae, numerical simulations may, in the first approximation, be conducted using conventional elements to represent the composite and replacing the interlaminar layer by interface elements. These have an appropriate evolution law of internal variables to simulate the failure process.

* Corresponding author. Tel.: +39-2-2399-4244; fax: +39-2-2399-4220.
E-mail address: coriglia@stru.polimi.it (A. Corigliano).

0020-7683/01/$ - see front matter
PII: S0020-7683(00)00088-3

When, as in the present paper, the phenomenon of delamination in polymer matrix composites is concerned, the viscous properties of the polymer can influence the global response to fracture and cause the type and extent of damage to depend on the time scale of load application (Popelar and Kanninen, 1980; Aliyu and Daniel, 1985; Smiley and Pipes, 1987; Friedrich et al., 1989; Hashemi et al., 1990). For example, the crack energy required to initiate and grow the delamination at any given speed, as well as the energy available at the crack tip, are functions of local visco-elastic properties, and significant load history effects may arise.

Experimental data obtained in Frassine et al. (1993, 1996) and Frassine and Pavan (1995), on two high-performance thermoplastic-matrix composites have shown that delamination fracture toughness may be remarkably rate sensitive, and that either increasing or decreasing values for increasing crack speed may be found.

To describe such behaviour using interface elements, the time dependence of the internal *damage law* has to be modified accordingly. Among all possible damage laws, which could reproduce the particular behaviour, one has to choose a law being consistent with the physics of the fracture process. An attempt has been done in Corigliano et al. (1997a,b, 1998), where the actual rate dependence of the yield stress of the matrix has been incorporated into the *damage law* of the interface model, by developing a viscoplastic softening interface law.

The main purposes of the present paper, which is the prosecution of the above referenced previously published works, are the following: formulate two time-dependent interface models to be used in the study of time-dependent delamination; describe in detail the behaviour of the models first by analytical computations, then by numerical integration of the governing equations; discuss the numerical implementation of the models in a finite-element non-linear analysis program; show the potentiality of the proposed modelling through finite element simulations of delamination crack propagation in interlaminar fracture specimens.

The summary of the paper is as follows: In Section 2, two time-dependent interface models are formulated; the first one is viscoplastic, while the second is time-dependent elastic damage. Section 3 concerns the computation of the analytical responses in pure mode of the proposed interface models; these are useful for comparison with the results of numerical implementation and for parameter identification. In Section 4, the numerical time integration of the interface models, carried out by means of a Runge–Kutta algorithm, is described; the numerical response of the models is studied at varying model parameters and loading conditions. The finite element implementation is discussed in Section 5, while in Section 6, some examples of numerical simulations of double cantilever beam and end notched flexure specimens are presented. Section 6 is concluded with a comparison between numerical and experimental results concerning a double cantilever beam test.

2. Formulation of two time-dependent interface models

The use of interface models for the simulation of fracture processes is becoming more and more popular. A typical context in which interfaces have recently been used is that of composite delamination. Other more complex fracture phenomena are those of fragmentation and impact, in those cases for some authors, the use of interfaces represents the only way to obtain a complete numerical simulation.

In this section, two interface models with a time-dependent response are proposed; they are formulated on the basis of previous works (Corigliano et al., 1997a,b, 1998) mainly for the simulation of time-dependent composite delamination (Aliyu and Daniel, 1985; Frassine et al., 1993); Frassine and paran, 1995); Friedrich et al., 1989). The model proposed could also be applied in other contexts, e.g. as done by Bažant and Beissel (1994), Satmani Naresh et al. (1996) and Netmes and Spéciel (1996).

Before starting the description of the models, it is worth specifying that an interface model is here conceived as a relation between the traction vector $\mathbf{t}$, relevant to a surface Γ, which separates a solid into

two parts Ω^+ and Ω^-, and the vector of displacement jumps or displacement discontinuities $[\mathbf{u}]$ representing the possible relative movements of the two parts of the solid (Fig. 1). The interface is therefore a useful schematisation for the introduction of displacement discontinuities, i.e. cracks, in the solid. Interface models can also be considered as generalisations of the cohesive crack concept.

When composite delamination is concerned, the laminate is conceived as a stacking sequence of layers and interfaces (Fig. 2), the interface acts as a zero-thickness medium which transfer stresses from one layer to the adjacent. The interface can have orthotropic properties, with the principal orthotropic directions depending on the fibre directions of adjacent layers (Fig. 2). With the above schematisation, it is possible to describe the behaviour of an interface zone with very small thickness and to attribute to it different mechanical responses.

The models introduced in Sections 2.1 and 2.2 are formulated following the reference frame of Fig. 2. Hence, traction in direction 3 activates a mode-I delamination mechanism, while tractions in directions 2 and 3 are related to mode II and III delamination, respectively.

2.1. Viscoplastic model

A viscoplastic interface model is first introduced, governed by the following relations:

$$[\mathbf{u}] = [\mathbf{u}]^{\mathrm{e}} + [\mathbf{u}]^{\mathrm{vp}}, \tag{1}$$

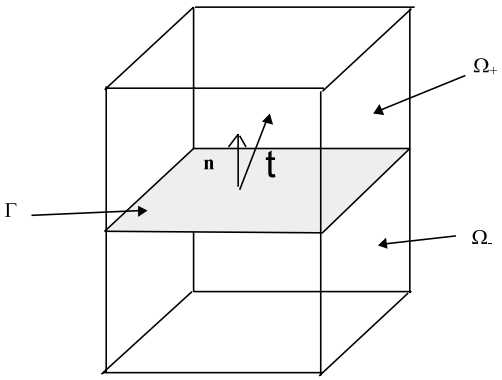

Fig. 1. Interface Γ in a solid Ω.

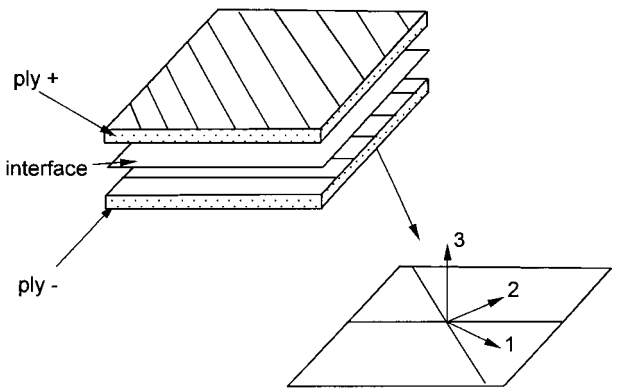

Fig. 2. Schematic representation of a laminate.

$$\mathbf{t} = \mathbf{K}[\mathbf{u}]^{\mathrm{e}}, \quad \mathbf{K} = \mathrm{diag}(K_i), \quad i = 1,2,3, \tag{2}$$

$$[\dot{\mathbf{u}}]^{\mathrm{vp}} = \gamma \langle f(\mathbf{t},\lambda)\rangle_+^N \frac{\partial f(\mathbf{t},\lambda)}{\partial \mathbf{t}}, \tag{3}$$

$$f(\mathbf{t},\lambda) = \sqrt{a_1 t_1^2 + a_2 t_2^2 + a_3 \langle t_3\rangle_+^2} - 1 + h\lambda, \tag{4}$$

$$\lambda = \int_0^\tau \sqrt{\left([\dot{\mathbf{u}}]^{\mathrm{vp}}\right)^{\mathrm{T}} \left([\dot{\mathbf{u}}]^{\mathrm{vp}}\right)}\, \mathrm{d}\tau', \tag{5}$$

$$\langle \bullet \rangle_+ = \bullet \text{ if } \bullet > 0 \ \langle \bullet \rangle_+ = 0 \text{ if } \bullet \leqslant 0. \tag{6}$$

In Eq. (1), the additivity of elastic $[\mathbf{u}]^{\mathrm{e}}$ and viscoplastic $[\mathbf{u}]^{\mathrm{vp}}$ (i.e. irreversible) displacement discontinuities is assumed. The elastic behaviour of the interface is governed by relations (2), where interface elastic stiffnesses K_i, with the dimension of a force over a length cube, are introduced. Relation (3) governs the evolution of viscoplastic displacement discontinuities through a law of Perzyna kind (Perzyna, 1966), where γ and N are model parameters. $f(\mathbf{t},\lambda)$ is a viscoplastic potential defined in Eq. (4), function of interface tractions t_i and of a viscoplastic multiplier λ, defined in Eq. (5), where τ denotes time. Parameters a_i are related to the values of tractions at the beginning of the inelastic behaviour, while parameter h govern the hardening or softening character of the model in point. Relations (6) clarify the meaning of the symbol $\langle \bullet \rangle_+$, positive part of $\bullet$. The positive part of the traction normal to the interface is introduced in Eq. (4) in order to take into account a unilateral effect, thus avoiding development of viscoplastic displacement discontinuities in the normal direction when the interface is compressed. In other words, the component $[\dot{\mathbf{u}}]_3^{\mathrm{vp}}$ of the viscoplastic displacement discontinuity rate vector is zero when traction t_3 is negative.

The interface model introduced depends on nine parameters, which have the following dimensions:

$$\begin{array}{llr} K_i\ [F/L^3], & a_i\ [L^4/F^2], & i = 1,2,3, \\ h\ [1/L], & \gamma\ [F/LT], & N, \end{array}$$

where F, L, T denote force, length and time, respectively.

In Fig. 3, the initial elastic domain is represented in the space of interface tractions. When the parameter h is positive, a softening effect is introduced in the model and progressive interface degradation can be

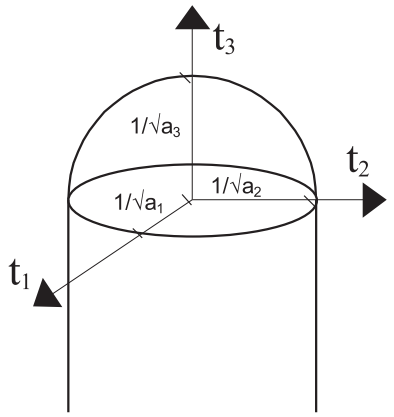

Fig. 3. Initial elastic domain for the viscoplastic interface.

described, this circumstance is exploited here in order to simulate delamination and debonding in composites.

2.2. Time-dependent damage model

As a possible alternative to the viscoplastic interface model above introduced, an anisotropic time-dependent elastic-damage model can be used, as defined by the following relations:

$$t_1 = (1 - D_1)K_1[u]_1, \qquad t_2 = (1 - D_2)K_2[u]_2, \tag{7a}$$

$$t_3 = (1 - D_3)K_3^+\langle[u]_3\rangle_+ + K_3^-\langle[u]_3\rangle_-, \tag{7b}$$

$$Y_1 = \tfrac{1}{2}K_1[u]_1^2, \qquad Y_2 = \tfrac{1}{2}K_2[u]_2^2, \qquad Y_3 = \tfrac{1}{2}K_3^+\langle[u]_3\rangle_+^2, \tag{8}$$

$$\hat{f}(\mathbf{Y}, \lambda) = \sqrt{\hat{a}_1 Y_1 + \hat{a}_2 Y_2 + \hat{a}_3 Y_3} - 1 + \hat{h}\lambda, \tag{9}$$

$$\dot{D}_i = \hat{\gamma}_i\left\langle \hat{f}(\mathbf{Y}, \lambda)\right\rangle_+^N, \quad i = 1, 2, 3, \tag{10}$$

$$\dot{\lambda} = \sqrt{\sum_{i=1}^{3}\dot{D}_i^2}. \tag{11}$$

Eq. (7) describe the elastic-damage behaviour of the interface; parameters K_i play the role of initial interface stiffnesses; D_i are three damage variables which affect the behaviour in the three different damage modes. It is to be noticed that in Eq. (7b), a unilateral effect in the direction 3 is introduced by distinguishing the elastic behaviour depending on the sign of the normal displacement discontinuity. For simplicity it will be assumed in the following: $K_3^+ = K_3^-$. The variables Y_i defined in Eq. (8) are energetically conjugate to the damage variables and coincide with the elastic energies associated to the single modes. The evolution of the three damage variables is governed by relations (9)–(11). In Eq. (9) the potential function $\hat{f}(\mathbf{Y}, \lambda)$ is defined, depending on $\mathbf{Y}$ and on the variable λ, which is a scalar measure of the total cumulated damage. Parameters $\hat{a}_i$ are related to the values of energies Y_i at the beginning of the inelastic behaviour, while parameter $\hat{h}$ influences the evolution of the function $\hat{f}(\mathbf{Y}, \lambda)$. The damage variables rates $\dot{D}_i$ are given in Eq. (10), where the positive part of $\hat{f}(\mathbf{Y}, \lambda)$ appears together with material parameters $\hat{\gamma}_i$ and N.

It is worth noticing that the above choice concerning the evolution of damage variables is a possibility among others. Eq. (10) defines the damage variables starting from the same potential, only the scalar multipliers $\hat{\gamma}_i$ are different for the three variables $\dot{D}_i$. This implies that the elastic stiffnesses are degraded in different proportions.

The damage interface model introduced above depends on nine parameters (when $K_3^+ = K_3^-$); these have now the following dimensions:

$$\begin{array}{lll} K_i\ [F/L^3], & \hat{a}_i\ [L/F], & i = 1, 2, 3, \\ \hat{h}, & \hat{\gamma}\ [1/T], & N. \end{array}$$

It is interesting to note that in the space of displacement discontinuities, the initial elastic domain has the same shape as that of the viscoplastic model in the space of interface tractions.

A softening effect, and therefore the possibility to describe progressive interface degradation, is introduced in the model provided that damage variables always increase, thus satisfying also a thermodynamical requirement. This last circumstance is verified if parameters $\hat{\gamma}$ are positive.

Both the interface models introduced above depend on nine model parameters. The large number of parameters and the consideration that direct tests on interfaces cannot be carried out, make the problem of parameter identification in the case of interface models a difficult task. In Corigliano (1993), Allix et al. (1995) and Allix and Corigliano (1996), the identification issues for interface problems have been already discussed. More recently, in Corigliano and Mariani (1999), an inverse approach based on the use of Kalman filter has been applied for the identification of time-dependent damage models.

In the present paper, model parameters are assumed to be known, in the case of parametric studies and purely numerical simulations, possibly found on the bases of the identification procedures described in the above referenced papers. In Section 6.3, a comparison between experimental and numerical results is shown and material parameter identification is briefly described.

3. Analytical response in pure mode

The response in pure mode for both models of Sections 2.1 and 2.2 can be obtained analytically for particular choices of parameters. This can be useful for the complete understanding of the model behaviour, for the purpose of parameter identification and for the validation of numerical procedures.

3.1. Viscoplastic model

The response of the viscoplastic interface model is sought for an assigned history of total displacement discontinuity $[u] = p(\tau)$, by specialising Eqs. (1)–(6) to the case of pure mode. Observe that a pure-mode response can be obtained by maintaining in Eqs. (1)–(5), one component of displacement discontinuity and traction only. Pure mode I, II or III are obtained by attributing to parameters a and K, the index 3, 1, 2, respectively (Fig. 2); in this and in the following section the index i will be dropped for brevity.

After the specialisation to pure-mode, a first-Order Differential Equation (ODE) can be obtained in the unknown viscoplastic displacement discontinuity $[u]^{\mathrm{vp}}$.

$$[\dot{u}]^{\mathrm{vp}} = \gamma\sqrt{a}\left(K\sqrt{a}p(\tau) - 1 - \left(K\sqrt{a} - h\right)[u]^{\mathrm{vp}}\right)^{N}. \tag{12}$$

In the special case $N = 1$, the above equation becomes linear and can be explicitly integrated; the result of the integration is given in the group of Eqs. (13) in the case of a linear history of total displacement discontinuity $p(\tau) = v\tau$.

$$\begin{aligned}
&N = 1, \quad [u](\tau) = p(\tau) = v\tau,\\
&\begin{cases} t(\tau) = Kv\tau, & 0 \leqslant \tau \leqslant \tau_0,\\ t(\tau) = C_1 \exp\left(C_4(\tau - \tau_0)\right) + C_2\tau + C_3, & \tau_0 \leqslant \tau \leqslant \tau_c, \end{cases}\\
&C_1 = -\frac{K^2 v}{\gamma\left(K\sqrt{a} - h\right)^2}, \qquad C_2 = -\frac{Kvh}{\left(K\sqrt{a} - h\right)},\\
&C_3 = \frac{K[Kv + \gamma(K\sqrt{a} - h)]}{\gamma\left(K\sqrt{a} - h\right)^2}, \qquad C_4 = -\gamma\sqrt{a}\left(K\sqrt{a} - h\right),\\
&\tau_0 = \frac{1}{Kv\sqrt{a}}, \quad \tau_c \cong -\frac{C_3}{C_2}.
\end{aligned} \tag{13}$$

At the limit, for the imposed velocity $v \to 0$, or for the viscosity parameter $\gamma \to \infty$, the response $t = t([u])$ in pure mode governed by relations in (13), obtained with $N = 1$, results in

$$t = t([u]) = \left(\frac{K}{K\sqrt{a} - h}\right)(1 - h[u]). \tag{14}$$

The above relation coincides with the response in pure mode of a time-independent elasto-plastic interface model governed by the following set of relations:

$$\begin{aligned} &t = K([u] - [u]^{\mathrm{vp}}), \qquad [\dot{u}]^{\mathrm{vp}} = \frac{\mathrm{d}F}{\mathrm{d}t}\dot{\lambda}, \\ &F = \sqrt{a}t - 1 + h\sqrt{a}\lambda \leqslant 0, \quad \dot{\lambda} \geqslant 0, \;\; F\dot{\lambda} = 0. \end{aligned} \tag{15}$$

The analytically computed response in pure mode of Eqs. (13) is shown at varying imposed velocity of displacement discontinuity in Fig. 4a, and at varying parameter h, for an imposed velocity of 0.1 mm/s, in Fig. 4b. The parameters chosen for the model are as follows:

$$\begin{aligned} &K = 100\,000\ \mathrm{N/mm^3}, \quad a = 1/80^2\ \mathrm{mm^4/N^2}, \quad h = 120\ \mathrm{mm^{-1}}, \\ &\gamma = 180\ \mathrm{N/mm\,s}, \quad N = 1. \end{aligned}$$

The above parameters are assumed to be a priori known, found on the bases of some identification procedure as those described in the papers referenced at the end of Section 2.

An important parameter for the behaviour of the model is the value of the area under the traction–displacement discontinuity plot; this in fact coincides with the fracture energy. As can be appreciated from Fig. 4a, the fracture energy predicted by the model increases at increasing imposed velocity of displacement discontinuity. Observe that at the limit for the imposed velocity $v \to 0$, the fracture energy with the above parameters is equal to 0.333 N/mm and coincides with that of the time independent model governed by Eq. (15). This value can be found by computing the area under the traction–displacement discontinuity plot in pure-mode response of the time-independent model (15), obtained applying a monotonically increasing history of displacement discontinuity.

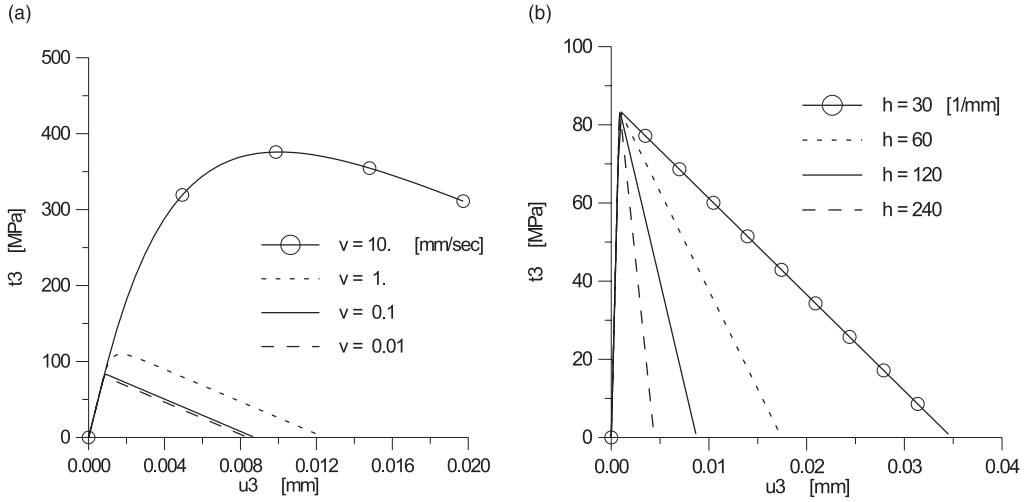

Fig. 4. Analytically computed traction–displacement discontinuity pure-mode response for the viscoplastic interface. (a) Response at varying imposed displacement discontinuity velocity, $h = 120\ \mathrm{mm^{-1}}$ (b) Response at varying parameter h, imposed velocity $v = 0.1$ mm/s.

3.2. Time-dependent damage model

As done for the viscoplastic model, the response of the time-dependent damage interface model is sought for assigned history of total displacement discontinuity $[u] = p(\tau)$; by specialising Eqs. (7)–(11) to the case of pure mode, a first-order differential equation can be obtained in the unknown scalar damage variable D:

$$\dot{D} = \hat{\gamma}\left(\sqrt{\frac{\hat{a}K}{2}}p(\tau) - 1 + \hat{h}D\right)^N. \tag{16}$$

When the parameter $N = 1$, the above equation reduces to a first-order linear ODE which can be explicitly integrated, the results are grouped in relations (17) shown below. Traction–displacement discontinuity in pure mode under monotonic loading for the damage model is as follows:

$$\begin{aligned}
&N = 1, \quad [u](\tau) = v\tau,\\
&\begin{cases} t(\tau) = Kv\tau, & 0 \leqslant \tau \leqslant \tau_0,\\ t(\tau) = C_1\tau\exp(C_4(\tau-\tau_0)) + C_2\tau^2 + C_3\tau, & \tau_0 \leqslant \tau \leqslant \tau_c, \end{cases}\\
&C_1 = -\frac{Kv^2}{\hat{\gamma}\hat{h}^2}\sqrt{\frac{\hat{a}K}{2}}, \qquad C_2 = \frac{Kv^2}{\hat{h}}\sqrt{\frac{\hat{a}K}{2}},\\
&C_3 = Kv\left(1 - \frac{1}{\hat{h}} + \frac{v}{\hat{\gamma}\hat{h}^2}\sqrt{\frac{\hat{a}K}{2}}\right), \qquad C_4 = \hat{\gamma}\hat{h},\\
&\tau_0 = \frac{1}{v}\sqrt{\frac{2}{\hat{a}K}}.
\end{aligned} \tag{17}$$

The expression of τ_c, i.e. the time instant corresponding to zero traction, is not given in Eq. (17), due to the fact that an explicit expression cannot be found easily. For low velocities and when $\hat{h} < 0$, a useful approximate expression is $\tau_c \cong -C_3/C_2$.

At the limit for the imposed velocity $v \to 0$, or for the viscosity parameter $\gamma \to \infty$, the response $t = t([u])$ in pure mode governed by relations in Eq. (17), obtained with $N = 1$, results in

$$t = t([u]) = K\left(1 - \frac{1}{\hat{h}}\left(1 - \sqrt{\frac{\hat{a}K}{2}}\right)[u]\right)[u]. \tag{18}$$

The above response coincides with that of a time-independent elastic-damage interface model governed by the following relations:

$$\begin{aligned}
&t = K(1-D)[u]. \quad Y = \tfrac{1}{2}K[u]^2,\\
&\hat{F} = \sqrt{\hat{a}Y} - 1 + \hat{h}D \leqslant 0, \quad \dot{D} \geqslant 0, \quad \hat{F}\dot{D} = 0.
\end{aligned} \tag{19}$$

The analytically computed response in pure mode is shown at varying imposed velocity of displacement discontinuity in Fig. 5a, while in Fig. 5b it is shown at varying parameter $\hat{h}$ for an imposed velocity $v = 0.1$ mm/s. The parameters chosen for the model are the following:

$$K = 100\,000 \text{ N/mm}^3, \quad \hat{a} = 31.25 \text{ mm/N}, \quad \hat{h} = -4, \quad \gamma = 180 \text{ 1/s}, \quad N = 1.$$

As noticed for the viscoplastic interface model, the above parameters are assumed to be a priori known, found on the bases of some identification procedure as those described in the papers referenced at the end of the previous section.

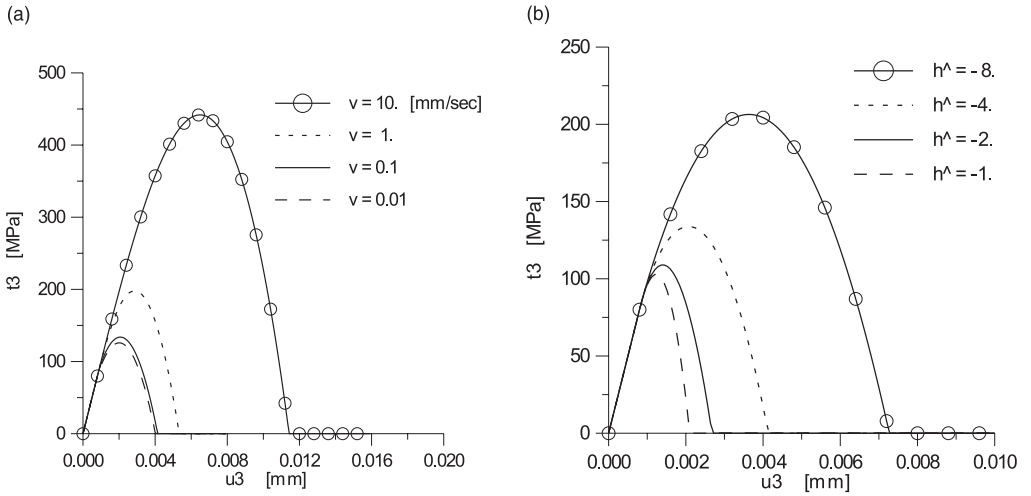

Fig. 5. Analytically computed traction–displacement discontinuity pure-mode response for the damage interface: (a) Response at varying imposed displacement discontinuity velocity $\hat{h} = -4$. (b) Response at varying parameter $\hat{h}$, imposed velocity $v = 0.1$ mm/s.

Note that with the above parameters, at the limit for the imposed velocity $v \to 0$, the fracture energy is equal to 0.333 N/mm and therefore coincides with that shown by the viscoplastic interface model of Fig. 4a and b.

The responses in Fig. 5a show clearly that the fracture energy strongly increases at increasing displacement discontinuity velocity.

4. Numerical time-integration

The interface models presented in Section 2 must be numerically integrated in time for their introduction in a non-linear step-by-step analysis.

The strategy here chosen is of a Runge–Kutta kind for both models of Sections 2.1 and 2.2 and is detailed in the following of this section.

The time history is subdivided in time steps $\Delta\tau = \tau_{n+1} - \tau_n$, at the beginning of each step all quantities are known. The solution of the single step consists in finding all unknown quantities at the time instant τ_{n+1} by giving as input the increment of the total displacement discontinuity in the step. Depending on the sign of a trial function f^{trial}, the step is elastic or non-linear. Indices n and $n+1$ denote quantities computed at time instants τ_n or τ_{n+1}, respectively.

4.1. Viscoplastic model

The elastic case is governed by the relations given below:

$$\begin{aligned} &\text{if } f(\mathbf{t}_n, \lambda_n) \leqslant 0 \\ &[\mathbf{u}]^{\text{vp}}_{n+1} = [\mathbf{u}]^{\text{vp}}_n; \quad \lambda_{n+1} = \lambda_n; \\ &\mathbf{t}_{n+1} = \mathbf{K}\big([\mathbf{u}]_{n+1} - [\mathbf{u}]^{\text{vp}}_n\big). \end{aligned} \tag{20}$$

The non-linear case implies the development of viscoplastic displacement discontinuities. A mid-point approximation governed by parameter ϑ is introduced for the unknowns viscoplastic displacement

discontinuity $[\mathbf{u}]^{\mathrm{vp}}_{n+1}$ and for the viscoplastic multiplier λ_{n+1}. The corresponding rate quantities $[\dot{\mathbf{u}}]^{\mathrm{vp}}_{n+1}$ and $\dot{\lambda}_{n+1}$ are expanded in a Taylor series up to the first order.

The resulting equations governing the non-linear phase for the time step are given here below:

$$
\begin{aligned}
&\text{if } f(\mathbf{t}_n, \lambda_n) > 0,\\
&\mathbf{t}_{n+1} = \mathbf{K}\big([\mathbf{u}]_{n+1} - [\mathbf{u}]^{\mathrm{vp}}_{n+1}\big),\\
&[\mathbf{u}]^{\mathrm{vp}}_{n+1} = [\mathbf{u}]^{\mathrm{vp}}_{n} + \Delta\tau\Big((1-\vartheta)[\dot{\mathbf{u}}]^{\mathrm{vp}}_{n} + \vartheta[\dot{\mathbf{u}}]^{\mathrm{vp}}_{n+1}\Big),\\
&\lambda_{n+1} = \lambda_n + \Delta\tau\Big((1-\vartheta)\dot{\lambda}_n + \vartheta\dot{\lambda}_{n+1}\Big), \quad \vartheta \in [0,1],\\
&[\dot{\mathbf{u}}]^{\mathrm{vp}}_{n+1} = [\dot{\mathbf{u}}]^{\mathrm{vp}}_{n} + \left(\frac{\partial[\dot{\mathbf{u}}]^{\mathrm{vp}}}{\partial \mathbf{t}}\bigg|_n\right)^{\mathrm{T}}\Delta\mathbf{t} + \left(\frac{\partial[\dot{\mathbf{u}}]^{\mathrm{vp}}}{\partial \lambda}\bigg|_n\right)^{\mathrm{T}}\Delta\lambda,\\
&\dot{\lambda}_{n+1} = \dot{\lambda}_n + \left(\frac{\partial\dot{\lambda}}{\partial[\dot{\mathbf{u}}]^{\mathrm{vp}}}\bigg|_n\right)^{\mathrm{T}}\Delta[\dot{\mathbf{u}}]^{\mathrm{vp}}.\\
&[\dot{\mathbf{u}}]^{\mathrm{vp}} = \gamma f^N(\mathbf{t},\lambda)\frac{\partial f}{\partial \mathbf{t}}, \quad \dot{\lambda} = \sqrt{[\dot{\mathbf{u}}]^{\mathrm{vp}^{\mathrm{T}}}[\dot{\mathbf{u}}]^{\mathrm{vp}}}.
\end{aligned}
\tag{21}
$$

By making use of Eqs. (21), it is possible to obtain an explicit expression for the traction vector $\mathbf{t}$ at the end of the time step (Appendix A)

$$
\mathbf{t}_{n+1} = \mathbf{t}_n + \mathbf{K}^*_n\Delta[\mathbf{u}] - \Delta\mathbf{q}_n. \tag{22}
$$

Matrix $\mathbf{K}^*_n$ and vector $\Delta\mathbf{q}_n$ in the above Eq. (22) are defined as follows:

$$
\mathbf{K}_{\mathrm{T}} \equiv \left(\frac{\partial\mathbf{t}_{n+1}}{\partial[\mathbf{u}]_{n+1}}\right)^{\mathrm{T}} = \mathbf{K}^*_n \equiv (\mathbf{I} + \Delta\tau\vartheta\mathbf{K}\mathbf{A}\mathbf{B})^{-1}\mathbf{K}, \tag{23a}
$$

$$
\mathbf{A} \equiv \left(I - \Delta\tau\vartheta\mathbf{C}\frac{\left([\dot{\mathbf{u}}]^{\mathrm{vp}}_n\right)^{\mathrm{T}}}{\dot{\lambda}_n}\right)^{-1}, \quad \mathbf{B} \equiv \left(\frac{\partial[\dot{\mathbf{u}}]^{\mathrm{vp}}}{\partial\mathbf{t}}\bigg|_n\right)^{\mathrm{T}}, \quad \mathbf{C} \equiv \left(\frac{\partial[\dot{\mathbf{u}}]^{\mathrm{vp}}}{\partial\lambda}\bigg|_n\right)^{\mathrm{T}}, \tag{23b, c}
$$

$$
\Delta\mathbf{q}_n \equiv \Delta\tau\mathbf{K}^*_n\Big([\dot{\mathbf{u}}]^{\mathrm{vp}}_n + \Delta\tau\vartheta\mathbf{A}\mathbf{C}\dot{\lambda}_n\Big). \tag{23d}
$$

Matrix $\mathbf{K}^*_n$ plays the role of tangent matrix, as specified in Eq. (23a).

In order to check the validity of the above integration procedure, in Fig. 6 a comparison is made between the numerically integrated response and the analytical results of Section 3.1 for the case $N = 1$. The two values 0 and 0.5 of the integration parameter ϑ are chosen. In Fig. 6a, the numerical response is computed with a time step $\Delta\tau = 0.001$ s, this corresponds to about 1/90 of the critical time instant, i.e. the instant corresponding to zero traction. It can be observed that the response for $\vartheta = 0$, i.e., a completely explicit one, is highly oscillating. The oscillations disappear in Fig. 6b where the numerical response is computed with a time step $\Delta\tau = 0.0001$ s, which corresponds to about 1/900 of the critical time step.

4.2. Time-dependent damage model

In the case of the time-dependent damage model, the elastic phase is governed by relations given below:

$$
\begin{aligned}
&\text{if } \hat{f}(\mathbf{Y}_n, \lambda_n) \leqslant 0,\\
&D_{i_{n+1}} = D_{i_n}, \quad \lambda_{n+1} = \lambda_n,\\
&\mathrm{t}_{in+1} = K_i(1 - D_{i_n})[u]_{i_{n+1}}, \quad Y_{i_{n+1}} = \tfrac{1}{2}K_i[u]^2_i, \ \ i = 1,2,3.
\end{aligned}
\tag{24}
$$

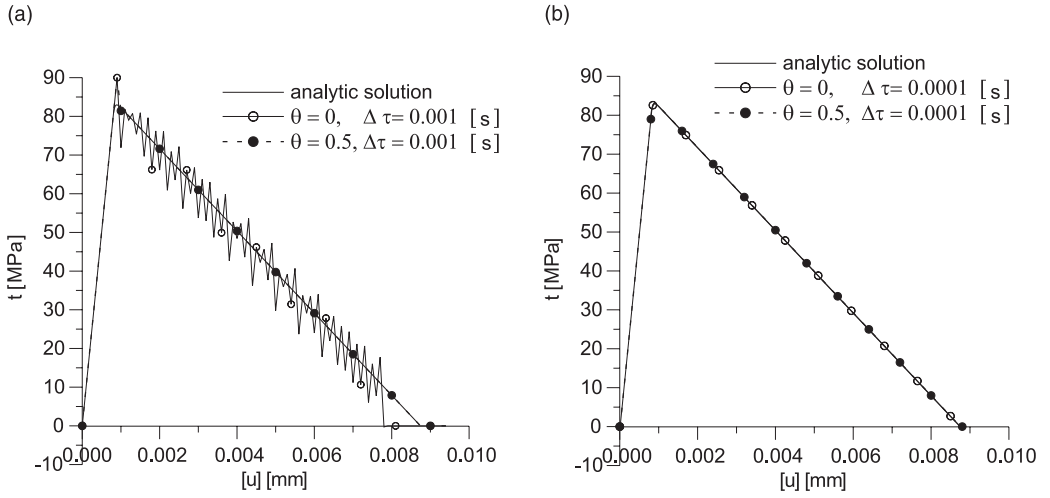

Fig. 6. Viscoplastic interface model. Comparison between analytic solution and numerical time integrated pure-mode response. Imposed displacement discontinuity velocity $v = 0.1$ mm/s: (a) 90 time steps and (b) 900 time steps.

The positive part $\langle [u]_3 \rangle_+$, which appears in Eqs. (7) and (8) for the purpose of modelling the unilateral effect, does not show up in this section only for notation convenience.

When the non-linear case is activated, damage variables evolve. In this case a mid-point approximation governed by parameter ϑ is introduced for the unknown damage variables $D_{i_{n+1}}$ and for the damage multiplier λ_{n+1}. A Taylor series expansion is used for their rate counterparts $\dot{D}_{i_{n+1}}$ and $\dot{\lambda}_{n+1}$. The resulting set of equations is given below; note that in Eq. (25), the three damage variables (and the corresponding rates) are collected in the diagonal matrices $\mathbf{D}_{n+1}(\dot{\mathbf{D}}_{n+1})$ for notation convenience. Elastic–viscoplastic case for the time-integrated viscoplastic model is as follows:

$$
\begin{aligned}
&\text{if } \hat{f}(\mathbf{Y}_n, \lambda_n) > 0,\\
&\mathbf{t}_{n+1} = (\mathbf{I} - \mathbf{D}_{n+1})\mathbf{K}[\mathbf{u}]_{n+1}, \quad \mathbf{D} \equiv \operatorname{diag}(D_i), \quad \mathbf{K} \equiv \operatorname{diag}(K_i), \ \ i = 1,2,3,\\
&\mathbf{D}_{n+1} = \mathbf{D}_n + \Delta\tau((1-\vartheta)\dot{\mathbf{D}}_n + \vartheta\dot{\mathbf{D}}_{n+1}),\\
&\lambda_{n+1} = \lambda_n + \Delta\tau((1-\vartheta)\dot{\lambda}_n + \vartheta\dot{\lambda}_{n+1}), \quad \vartheta \in [0,1],\\
&\dot{\mathbf{D}}_{n+1} = \dot{\mathbf{D}}_n + \left(\left.\frac{\partial\dot{\mathbf{D}}}{\partial\mathbf{Y}}\right|_n\right)^{\mathrm{T}} \Delta\mathbf{Y} + \left(\left.\frac{\partial\dot{\mathbf{D}}}{\partial\lambda}\right|_n\right)^{\mathrm{T}} \Delta\lambda,\\
&\dot{\lambda}_{n+1} = \dot{\lambda}_n + \left(\left.\frac{\partial\dot{\lambda}}{\partial\dot{\mathbf{D}}}\right|_n\right)^{\mathrm{T}} \Delta\dot{\mathbf{D}},\\
&\dot{D}_i = \hat{\gamma}_i \hat{f}(\mathbf{Y}, \lambda)^N, \quad i = 1,2,3, \ \ \dot{\lambda} = \sqrt{\sum_{i=1}^{3} \dot{D}_i^2}.
\end{aligned}
\tag{25}
$$

The direct exploitation of relations in Eq. (25), gives the following explicit format for the response in the time step (Appendix B).

$$
\mathbf{t}_{n+1} = (\mathbf{I} - \mathbf{D}_{n+1})\mathbf{K}[\mathbf{u}]_{n+1}, \tag{26}
$$

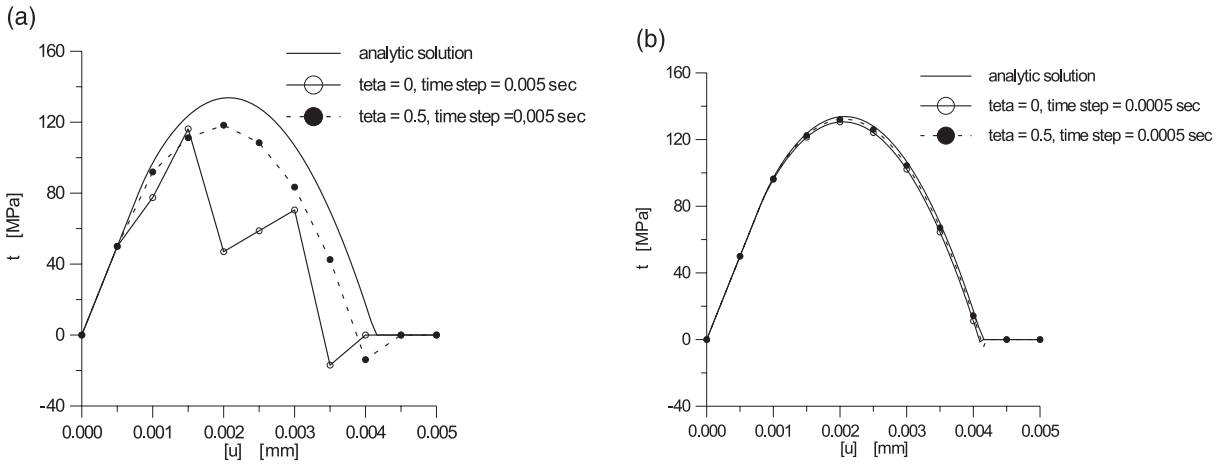

Fig. 7. Time-dependent damage interface model. Comparison between analytic solution and numerical time integrated pure-mode response. Imposed displacement discontinuity velocity $v = 0.1$ mm/s: (a) nine time steps and (b) 90 time steps.

where

$$\mathbf{D}_{n+1} = \mathbf{D}_n + \Delta\tau\left(\dot{\mathbf{D}}_n + \vartheta\hat{\mathbf{A}}\hat{\mathbf{B}}\Delta\mathbf{Y} + \vartheta\Delta\tau\hat{\mathbf{A}}\hat{\mathbf{C}}\dot{\lambda}_n\right), \tag{27a}$$

$$\hat{\mathbf{A}} \equiv \left(\mathbf{I} - \Delta\tau\vartheta\hat{\mathbf{C}}\frac{\left(\dot{\mathbf{D}}_n\right)^{\mathrm{T}}}{\dot{\lambda}_n}\right)^{-1}, \quad \hat{\mathbf{B}} \equiv \left(\frac{\partial\dot{\mathbf{D}}}{\partial\mathbf{Y}}\bigg|_n\right)^{\mathrm{T}}, \quad \hat{\mathbf{C}} \equiv \left(\frac{\partial\dot{\mathbf{D}}}{\partial\lambda}\bigg|_n\right)^{\mathrm{T}}. \tag{27b, c}$$

In the present case, the derivation of the tangent matrix is not straightforward; its expression is given by the following equation:

$$\mathbf{K}_{\mathrm{T}} \equiv \left(\frac{\partial\mathbf{t}_{n+1}}{\partial[\mathbf{u}]_{n+1}}\right)^{\mathrm{T}} = \left((\mathbf{I} - \mathbf{D}_{n+1})\mathbf{K} - \Delta\tau\vartheta\left(\frac{\partial\mathbf{Y}_{n+1}}{\partial[\mathbf{u}]_{n+1}}\right)^{\mathrm{T}}\mathbf{A}\mathbf{B}\left(\frac{\partial\mathbf{Y}_{n+1}}{\partial[\mathbf{u}]_{n+1}}\right)\right). \tag{28}$$

A comparison between the numerically integrated response of the damage interface model and the analytical response of Section 3.2, is shown in Fig. 7 for the case $N = 1$. In Fig. 7a, a time step $\Delta\tau = 0.005$ s is used, which corresponds to about 1/9 of the critical time step; in Fig. 7b a time step 10 times smaller is used. From Fig. 7a, the advantage of making use of a mid-point approximation is evidenced.

4.3. Models behaviour and comparisons

A parametric study concerning the behaviour of the two proposed interface models is presented here; the results are obtained by means of the numerical integration procedures described in the Sections 4.1 and 4.2. If not specified differently, the set of parameters used for the two models are those of Sections 3.1 and 3.2, apart from the exponent N, which is now taken $N = 10$ in both cases.

The results concerning the behaviour of the viscoplastic model are shown in Figs. 8–12.

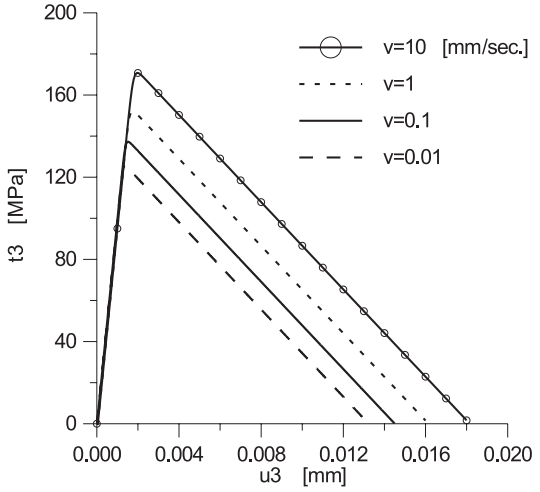

Fig. 8. Viscoplastic interface model: response in pure mode at varying displacement discontinuity velocity.

In Fig. 8, the pure mode response at varying imposed displacement discontinuity velocity is shown. By comparing this figure with Fig. 4a, obtained analytically for $N = 1$, it can be observed that with $N = 10$, the sensitivity to the value of imposed velocity is strongly reduced.

Fig. 9a–c concerns the pure-mode response at varying parameters h, γ and N, respectively, for an imposed displacement discontinuity velocity $v = 0.1$ mm/s. As already shown by Fig. 4b, the softening effect increases at increasing parameter h; γ and N, which govern the viscoplastic evolution law influence the value of fracture energy at fixed velocity.

Fig. 10a–c shows the difference in the model response for pure mode I and pure mode II. By imposing the cyclic displacement discontinuity history of Fig. 10a, the response in mode I is as in Fig. 10b, where the unilateral effect for negative values of traction is put in evidence, while the response in mode II is that in Fig. 10c.

For the models under discussion it is interesting to show the response under mixed-mode conditions. For the viscoplastic model, this is done in Fig. 11. Mixed-mode conditions have been obtained by applying monotonically increasing displacement discontinuity histories both in direction 1 (mode II) and in direction 3 (mode I) with a displacement discontinuity velocity in direction 3 fixed to the value $v_3 = 0.1$ mm/s and different velocities in direction 1. In the figure, only the behaviour in direction 3 is shown at varying value of velocity v_1 i.e. at varying *mixity ratios*. It can be appreciated from Fig. 11 that there is an increasing negative interaction effect at increasing mixity ratio; this and other items related to the behaviour of interface models in mixed-mode conditions have been discussed in Allix and Corigliano (1996).

As already observed, the fracture energy is a fundamental parameter for the interface model. In the present time-dependent context, it is in particular important to study the variation of the fracture energy with the imposed displacement discontinuity velocity. This is done in Fig. 12, where the fracture energy G_c is plotted versus the imposed displacement discontinuity velocity for the two values $N = 1$ and $N = 10$ in a semi-logarithmic diagram. The plots in Fig. 12 confirm what was already observed from Fig. 4a: when $N = 1$ the variation of fracture energy is extremely rapid.

Figs. 13–17 show the response of the time-dependent damage model, similar to Figs. 8–12 relevant to the viscoplastic model. Comments analogous to those already done with reference to Figs. 8–12 still apply. The main qualitative difference between the two models concerns the response to cyclic loading, shown in

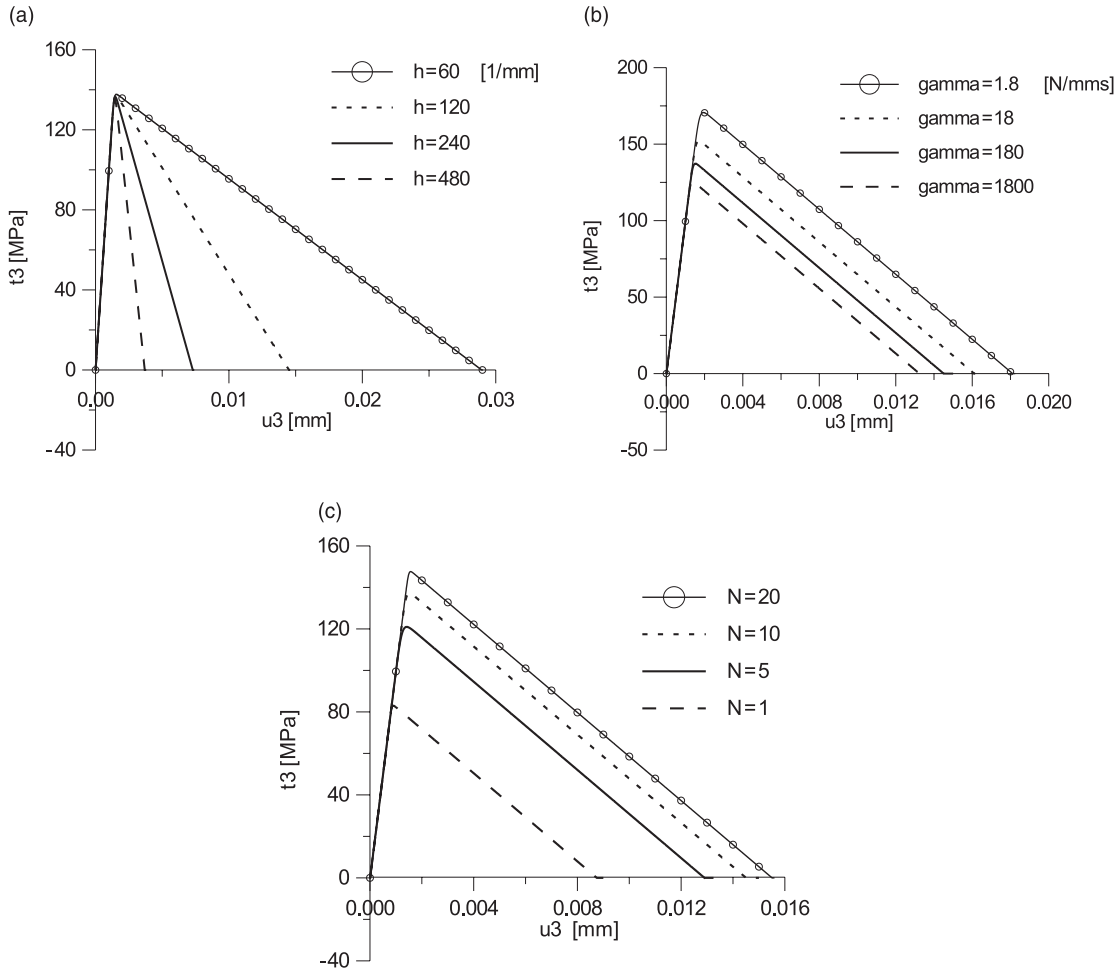

Fig. 9. Viscoplastic interface model – response in pure mode at varying model parameters: (a) h, (b) γ, and (c) N. Imposed displacement discontinuity velocity $v = 0.1$ mm/s.

Fig. 15a–c. From Fig. 15b, the unilateral effect can still be appreciated, while residual displacement discontinuities are obviously absent.

5. Finite element formulation

Interface models, as those discussed in Sections 2–4, can be introduced in a finite element formulation in order to obtain a numerical model of the structure or material under consideration.

A possible scheme, adopted here, is that of an elastic continuum Ω with non-linear interfaces Γ (Bolzon and Corigliano, 1997); in this case, the material non-linearities are all concentrated along the interfaces whose behaviour is governed by an interface model. This schematisation applied to delamination consists in considering elastic layers separated by non-linear interfaces.

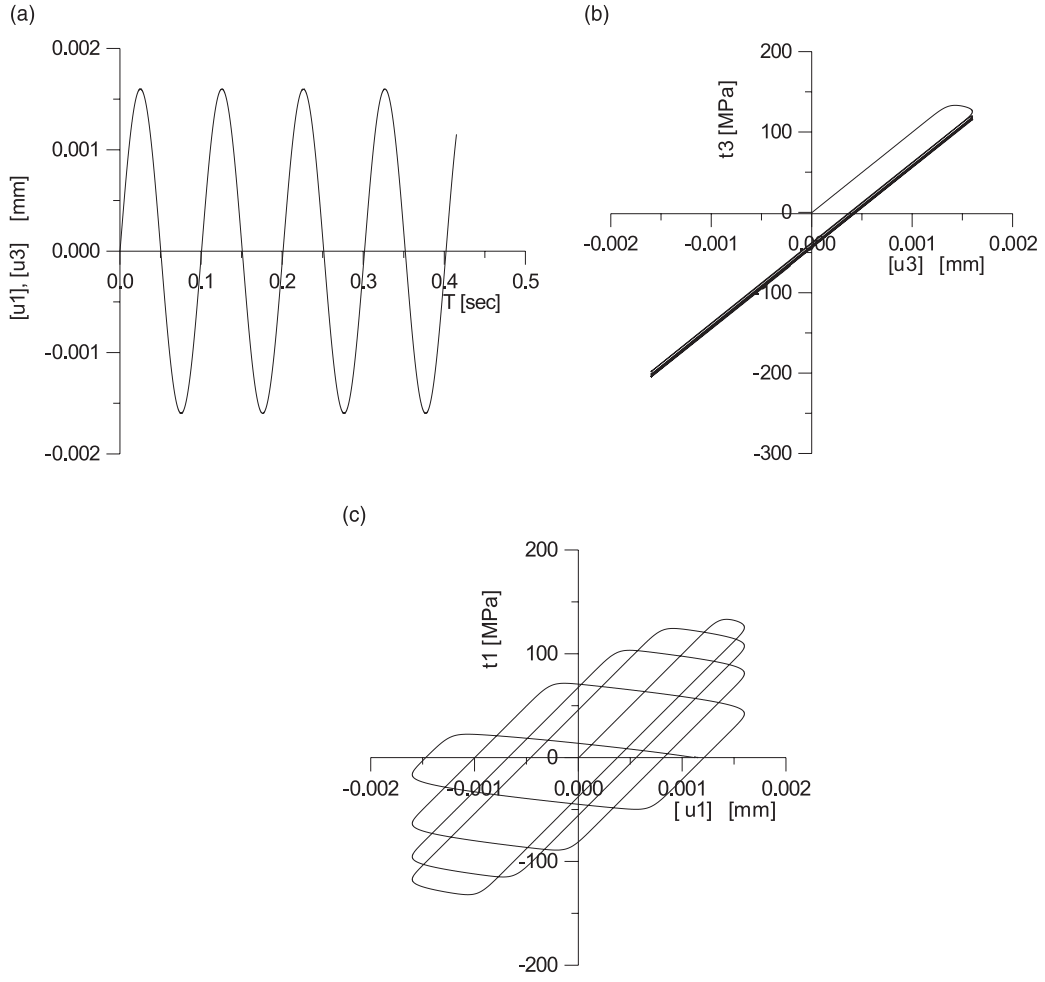

Fig. 10. Viscoplastic interface model – cyclic response in pure-modes I and II: (a) imposed displacement discontinuity history, (b) cyclic response in pure mode I with unilateral effect and (c) cyclic response in pure mode II.

After space and time discretisation, the equilibrium conditions at time instant τ_{n+1} can be formally written as

$$\mathbf{S}_{\Omega}\mathbf{U}_{n+1} + \int_{\Gamma} \mathbf{B}_{\Gamma}^{\mathrm{T}}\mathbf{t}_{n+1}\,\mathrm{d}\Gamma = \mathbf{P}_{n+1}, \tag{29}$$

where $\mathbf{S}_{\Omega}$ is the elastic stiffness matrix of the continuum part of Ω (the layers in a laminate), $\mathbf{B}_{\Gamma}$ represents the operator which relates interface displacement discontinuities $[\mathbf{u}]_{n+1}$ to the global nodal displacement vector $\mathbf{U}_{n+1}$, while $\mathbf{P}_{n+1}$ are equivalent nodal loads.

The global non-linear equilibrium equation (29) must be solved at each time step; the non-linearity comes from the non-linear dependence of the interface tractions $\mathbf{t}_{n+1}$ on the displacement discontinuities $[\mathbf{u}]_{n+1}$ as governed by the interface model numerically integrated in time. Typically Eq. (29) can be solved by means of the Newton–Raphson iterative method; at each iteration the following linear system of equations in the unknown $\mathbf{U}_{n+1}^{i+1}$ must be solved having determined all the quantities at iteration i:

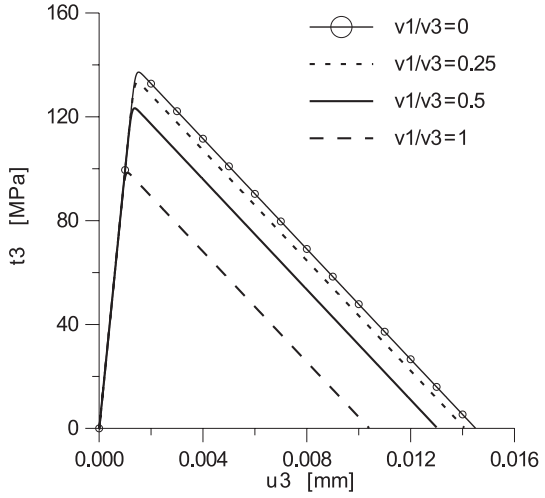

Fig. 11. Viscoplastic interface model: mixed-mode response.

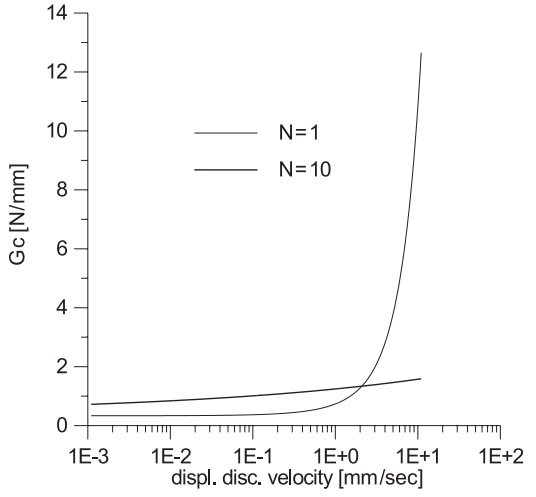

Fig. 12. Viscoplastic interface model: fracture energy as a function of the imposed displacement discontinuity velocity.

$$\left(\mathbf{S}_{\Omega}+\mathbf{S}^{i}_{\Gamma n+1}\right)\left(\mathbf{U}^{i+1}_{n+1}-\mathbf{U}^{i}_{n+1}\right)=\mathbf{P}_{n+1}-\mathbf{S}_{\Omega}\mathbf{U}^{i}_{n+1}-\int_{\Gamma}\mathbf{B}^{\mathrm{T}}_{\Gamma}\mathbf{t}^{i}_{n+1}\,\mathrm{d}\Gamma, \tag{30a}$$

$$\mathbf{S}^{i}_{\Gamma n+1}\equiv\int_{\Gamma}\mathbf{B}^{\mathrm{T}}_{\Gamma}\left(\frac{\partial\mathbf{t}_{n+1}}{\partial[\mathbf{u}]_{n+1}}\right)^{\mathrm{T}}\mathbf{B}_{\Gamma}\,\mathrm{d}\Gamma. \tag{30b}$$

Matrix $\mathbf{S}^{i}_{\Gamma n+1}$ defined above is the contribution to the global tangent matrix deriving from the interfaces. In order to compute $\mathbf{S}^{i}_{\Gamma n+1}$, the material tangent matrix relevant to the interface model must be computed, as done in Sections 4.1 (Eq. (23a)) and 4.2 (Eq. (28)) for the viscoplastic and time dependent damage models, respectively.

It is interesting to note that, in the case of the viscoplastic model of Section 4.1, the tangent matrix (Eq. (23a)) does not change during the iteration process because it depends on quantities computed at the be-

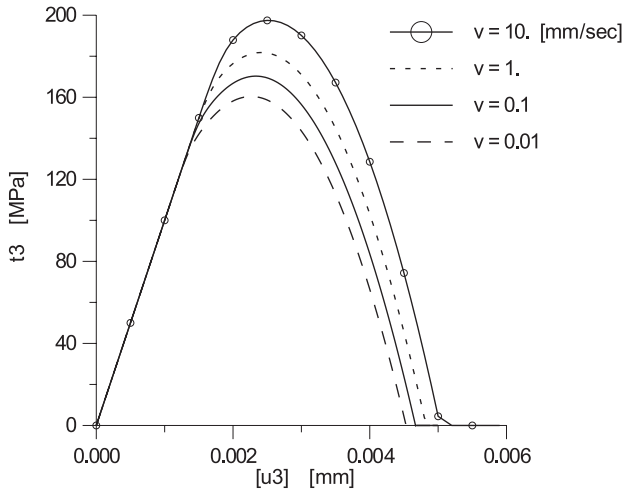

Fig. 13. Time-dependent damage interface model: response in pure mode at varying displacement discontinuity velocity.

ginning of the step, moreover the traction vector is explicitly computed (Eq. (22)). These circumstances transform the Newton–Raphson procedure in a simple explicit computation for the step, without any iteration:

$$(\mathbf{S}_{\Omega}+\mathbf{S}_{\Gamma n})\,\Delta\mathbf{U}=\mathbf{P}_{n+1}-\int_{\Omega}\mathbf{B}_{\Omega}^{\mathrm{T}}\sigma_n\,\mathrm{d}\Omega-\int_{\Gamma}\mathbf{B}_{\Gamma}^{\mathrm{T}}\mathbf{t}_n\,\mathrm{d}\Gamma+\int_{\Gamma}\mathbf{B}_{\Gamma}^{\mathrm{T}}\Delta\mathbf{q}_n\,\mathrm{d}\Gamma, \tag{31a}$$

$$\mathbf{S}_{\Gamma n}\equiv\int_{\Gamma}\mathbf{B}_{\Gamma}^{\mathrm{T}}\mathbf{K}_n^{*}\mathbf{B}_{\Gamma}\,\mathrm{d}\Gamma. \tag{31b}$$

The numerical finite element simulations presented in Section 6 are based on the above procedure; use is made of plane strain four node isoparametric elements, coupled with four nodes interface elements.

6. Numerical applications

In this section, numerical simulations of double cantilever beam (DCB) and end notched flexure (ENF) tests are presented (Fig. 18), based on the viscoplastic interface constitutive law of Section 2.1 and the finite element model of Section 5. Analogous simulations carried out by means of the damage law of Section 2.2, together with a detailed discussion concerning the numerical implementation and the comparison between experiments and simulations will be presented in a forthcoming paper.

6.1. Double cantilever beam simulation

The DCB specimen considered is shown in Fig. 19a, its dimensions are assumed as follows:

$$L=20\text{ mm},\quad H=1\text{ mm},\quad a_0=5\text{ mm},$$

where a_0 denotes the initial crack length.

The response of the specimen at imposed opening displacement velocity $v=1$ mm/s is first computed at varying mesh size. The four meshes of Fig. 19 are considered with the interface viscoplastic model of Section 2.1 and the interface model parameters used in Section 4.3. The two arms of the specimen are

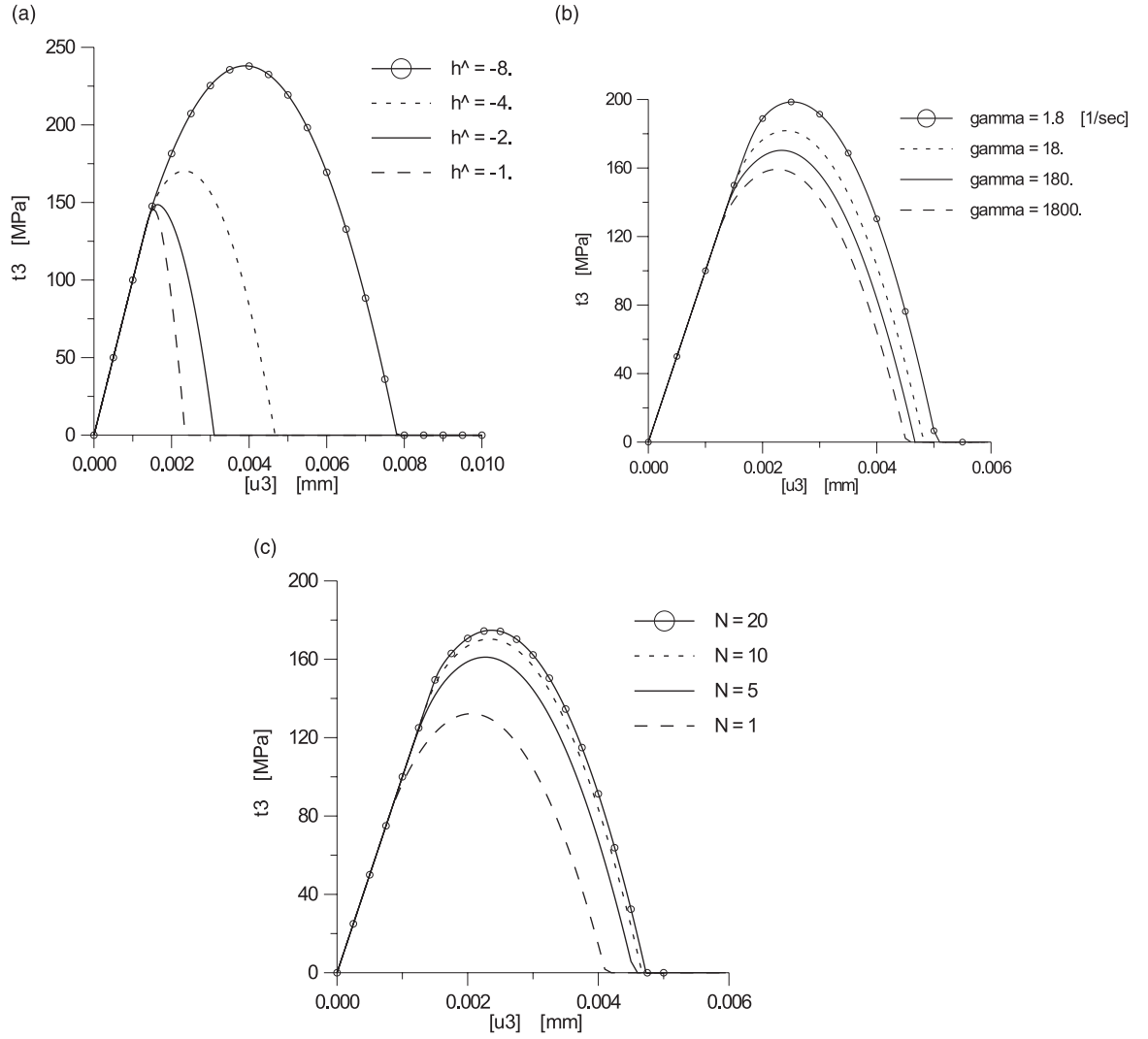

Fig. 14. Time-dependent damage interface model: response in pure mode at varying model parameters: (a) $\hat{h}$, (b) $\hat{\gamma}$, and (c) N. Imposed displacement discontinuity velocity $v = 0.1$ mm/s.

assumed to have an elastic, transversely isotropic behaviour governed by the following parameters in the reference frame of Fig. 19

$$E_{11} = 84\,766 \text{ MPa}, \quad E_{33} = 0.1E_{11},$$
$$G_{13} = 1000 \text{ MPa}, \quad \nu_{13} = 0.035, \quad \nu_{32} = 0.35.$$

The above parameters have been found on the bases of experimental results used for the comparison with numerical simulations in previous papers of the first author (Corigliano et al., 1997a,b, 1998), they are used here for numerical simulations only.

The four meshes used have elements measuring in the crack propagation direction 1, 0.5, 0.25, 0.125 mm, respectively, with the element-length/beam-length ratios L_e/L marked in the figure caption.

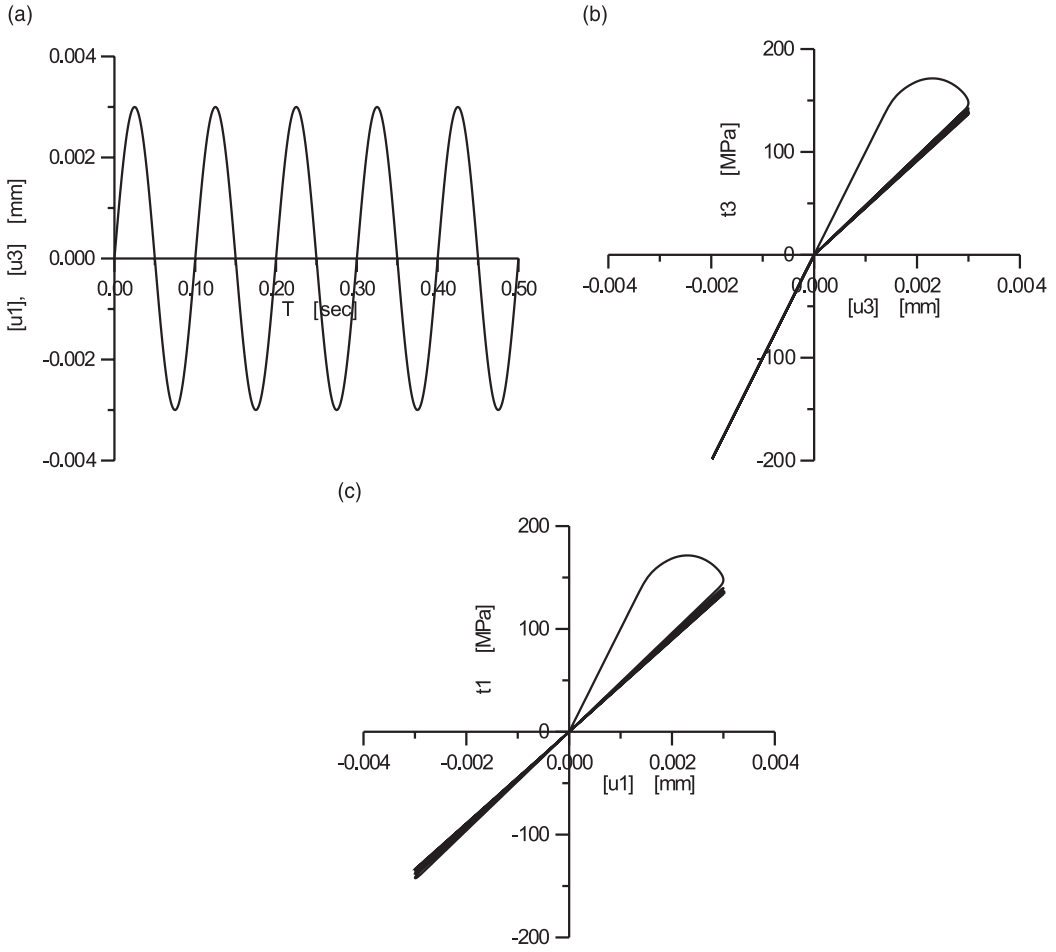

Fig. 15. Time-dependent damage interface model – cyclic response in pure modes I and II: (a) imposed displacement discontinuity history, (b) cyclic response in pure mode I with unilateral effect and (c) cyclic response in pure mode II.

In Fig. 20a, b, the response of the DCB obtained with the four meshes is shown in terms of the load–displacement plots and of the interlaminar traction t_3 along the interface. From a combined examination of the two figures, it can be concluded that the strong over-estimation of the response obtained with the coarser mesh is due to the fact that the interlaminar stress distribution is not correctly reproduced, in particular the high stress concentration at the crack tip. The necessity to use *small* elements when the interface schematisation used is well known (Schellekens and De Borst, 1993) and can be considered as one of the main drawbacks related to its application.

The response of the DCB specimen is then computed at varying imposed opening displacement velocity, with the finer mesh among those of Fig. 19. The results in term of the displacement–load plots are shown in Fig. 21. The plots in Fig. 21 increase with the imposed velocity, this is a consequence of the increase of fracture energy as given by the interface models.

As shown in the above example, mesh dependence is shown in the response of the specimen until when the element size is small enough to correctly reproduce the interlaminar stresses. For element size smaller than the above one, no pathological mesh dependence is shown.

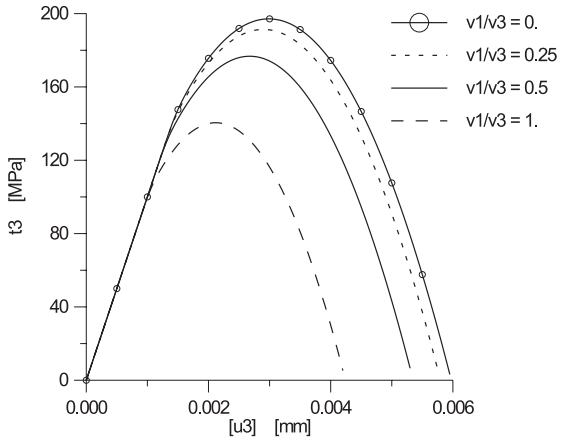

Fig. 16. Time-dependent damage interface model: mixed-mode response.

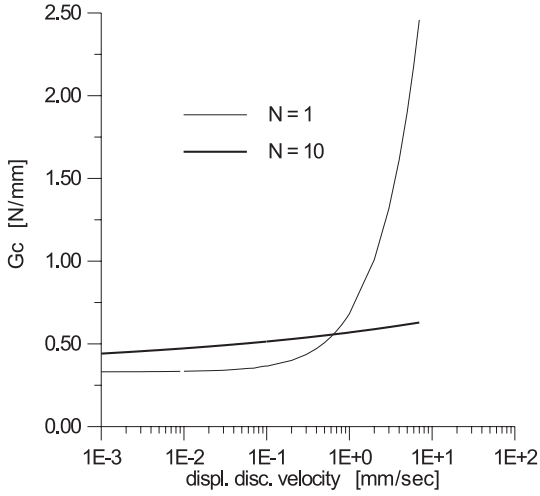

Fig. 17. Time-dependent damage interface model: fracture energy as a function of the imposed displacement discontinuity.

The important issue of pathological mesh dependence remains an open question for three-dimensional fracture phenomena described through interface elements.

6.2. End notched flexure simulation

The ENF specimen (Fig. 18b) considered for the simulation has the same dimensions of the DCB specimen analysed in the previous Section 6.1. The specimen is simply supported and the load is applied vertically downward at the centre of the upper arm. It is important to note that the simulation of the ENF test can be carried out due to the fact that a unilateral effect is introduced in the interface model, which avoids the superposition of the two arms.

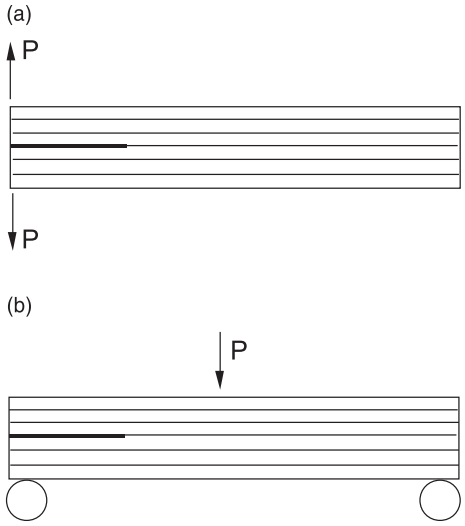

Fig. 18. Interlaminar fracture specimens: (a) DCB and (b) ENF.

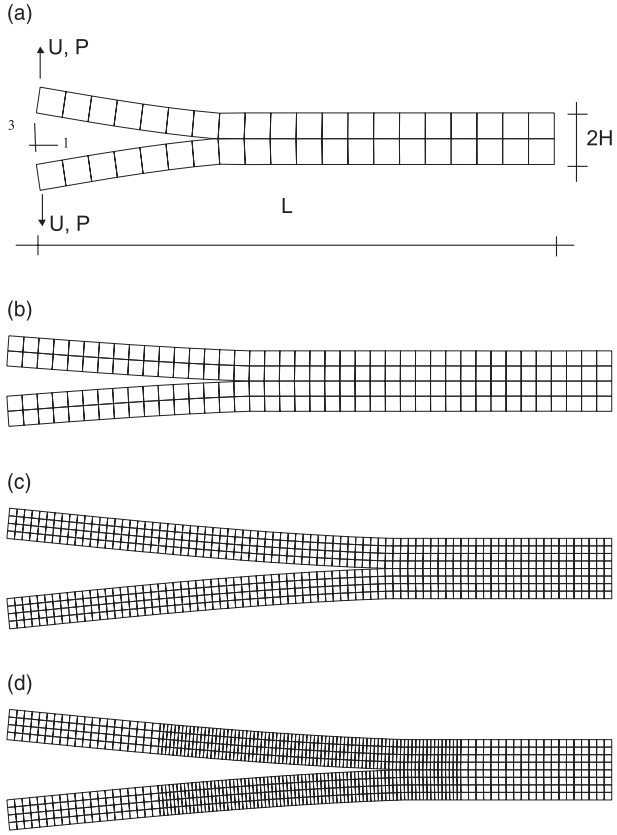

Fig. 19. Viscoplastic interface model – response of a DCB test at varying mesh size. The three meshes used: (a) $L_e/L = 0.05$, (b) $L_e/L = 0.025$, (c) $L_e/L = 0.0125$, (d) $L_e/L = 0.00625$.

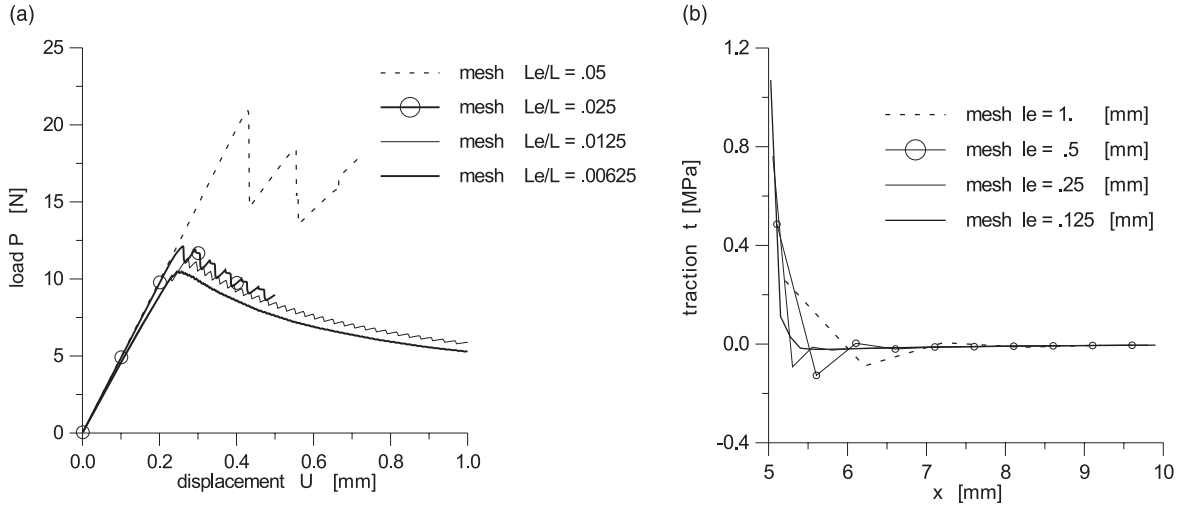

Fig. 20. Viscoplastic interface model – response of a DCB test at varying mesh size. Opening displacement velocity $v = 1$ mm/s: (a) load displacement plots and (b) traction distribution along the interface.

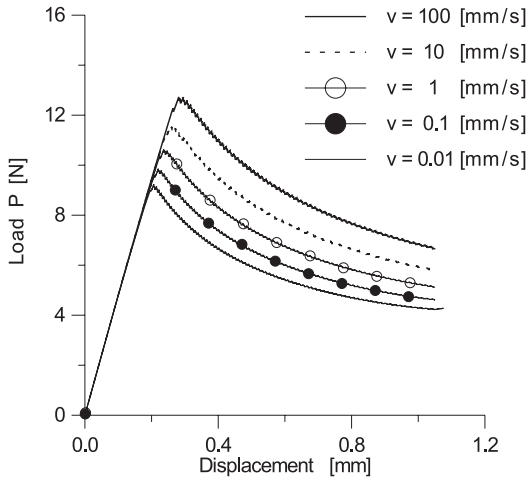

Fig. 21. Viscoplastic interface model: load displacement plots of a DCB test at varying imposed velocity of displacement.

The viscoplastic interface model is used for the simulation with the same set of parameters of Section 4.3. The behaviour of the two arms of the specimen is assumed to be elastic, transversely isotropic as in the previous Section 6.1.

The response of the specimen at varying velocity of imposed displacement in the loaded point is shown in Fig. 22a. As in the DCB simulations, it can be appreciated the increase with velocity of the energy dissipated during crack propagation, due to the increase of fracture energy as modelled by the interface law. It is also worth noting that the response of the specimen can be divided in three main parts: an elastic part with increasing load, a softening branch corresponding to crack propagation, a part with increasing load corresponding to the response after the delamination crack has passed the beam half. A simple explanation of

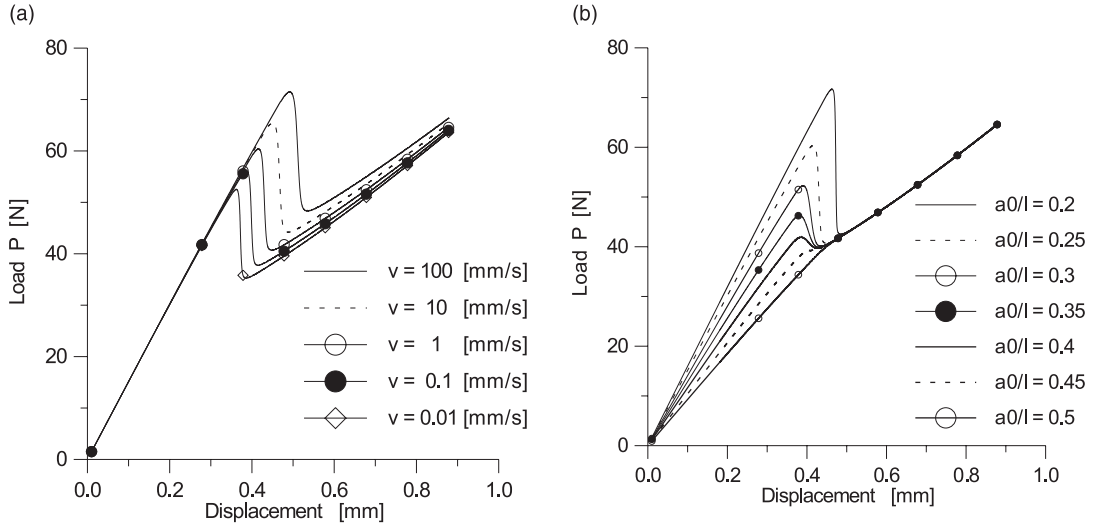

Fig. 22. Viscoplastic interface model – displacement–load plots in a ENF test: (a) at varying imposed velocity of displacement and (b) at varying initial crack length for imposed displacement velocity $v = 1$ mm/s.

this behaviour can be given on the basis of a linear elastic fracture mechanic model of the ENF test. This has been done in Allix et al. (1995) starting from the Griffith condition for crack propagation expressed in terms of the beam compliance. In a few words, it can be said that the response of the specimen have as a limit the linear elastic response of two superposed beams (the two arms of the specimen) without interlaminar connections, this is reached when complete delamination in mode II has occurred.

The ENF specimen is then analysed at varying initial crack length. As already discussed in Allix et al. (1995) and Allix and Corigliano (1996), the response of the specimen can be unstable also when the displacement is imposed (*snap-back* response) if initial crack length is sufficiently *small*. In Fig. 22b, the load–displacement plots, obtained for a velocity of imposed displacement $v = 1$ mm/s, show that when $a_0/L < 0.35$ the response tends to show snap-back; this is in agreement with the critical theoretical value $a_0/L = 0.347$ found in Allix et al. (1995).

6.3. Double cantilever beam test: comparison between numerical and experimental responses

The numerical model proposed in Sections 2–5 for the simulation of time-dependent interlaminar fracture is here applied to the simulation of a DCB carbon fibre-Poly Ether-Imide (PEI) composite specimen.

Frassine et al. (1993, 1996) and Frassine and Pavan (1995) obtained results concerning the behaviour of DCB specimens at varying velocity and temperature. They considered 16-ply unidirectional laminates 0.3 mm thick with PEI resin and carbon fibres and carried out interlaminar fracture tests on DCB specimens 20 mm wide and 170 mm long, having an initial crack length of 60 mm, following the ESIS protocol (Davies, 1992). The thickness varies between 3.6 and 4.2 mm, depending on the moulding conditions. The range of crack propagation velocities considered was such that dynamic crack effects were negligible.

By using for composites the time-temperature equivalence postulate valid for most polymers (Ferry, 1980), they obtained the plots of the fracture toughness G_c of the composite and of the neat resin shown in Fig. 23 (Corigliano et al., 1998). From Fig. 23, an increase of the composite fracture toughness with crack

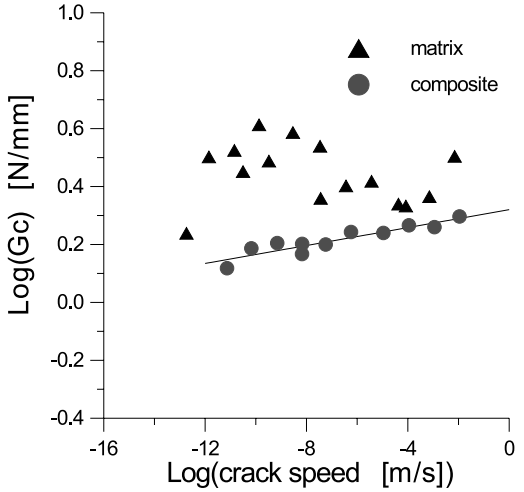

Fig. 23. Fracture toughness of the PEI matrix and of the composite versus crack speed master curve at $T_0 = 23°C$. The line represent power-law least square fitting. Experimental results from Frassine and Pavan (1995).

propagation velocity can be appreciated, while no clear dependence of the neat resin fracture toughness with the crack velocity can be observed.

The above experimental results have motivated the application of time-dependent interface models for the simulation of the DCB specimen at varying velocity (Corigliano et al., 1997a,b, 1998). A simulation of the test conducted by the above referenced authors is presented here in order to show the potentialities of the numerical model proposed in the present paper.

The schematisation used for the DCB specimen is as that presented in Section 6.1, with the same parameters for the elastic arms. The viscoplastic interface model has been used with the following set of parameters:

$$K = 200\,000\ \mathrm{N/mm^3}, \quad a = 1/60^2\ \mathrm{mm^4/N^2}, \quad h = 70\ \mathrm{mm^{-1}},$$
$$\gamma = 7\ \mathrm{N/mms}, \quad N = 16.$$

The above parameters have been identified, as suggested in (Corigliano et al., 1998), partially from the properties of the neat resin and partially starting from a direct comparison of the numerical and experimental load–displacement plots. More precisely, the interface elastic stiffness has been obtained starting from the elastic modulus of the resin:

$$K \cong \frac{E}{e}, \quad E = 3000\ \mathrm{MPa}, \quad e = 0.015\ \mathrm{mm},$$

where e is the thickness attributed to the interlaminar resin-rich region where the delamination process takes place. The parameter a has been linked to the value t_0 of traction corresponding to the onset of yielding in pure mode of the resin

$$a = \frac{1}{t_0^2}, \quad t_0 = 60\ \mathrm{MPa}.$$

As far as the parameters h, γ and N are concerned, they have been identified by directly matching the numerical and experimental global load–displacement plots for an imposed opening displacement velocity $v = 500$ mm/min.

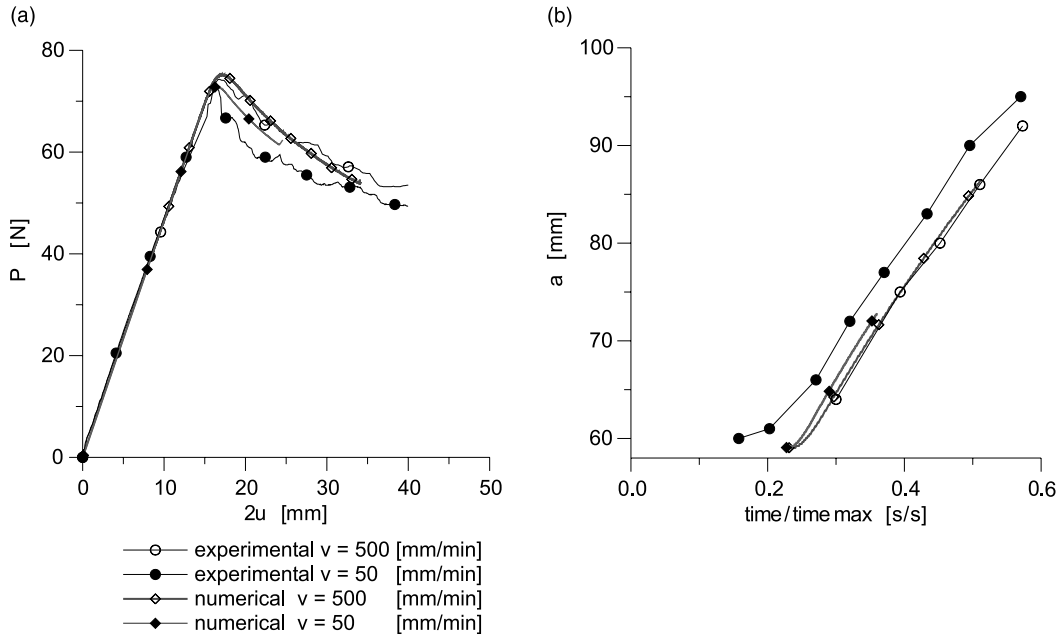

Fig. 24. DCB specimen. Experimental versus numerical responses: (a) load–displacement and (b) fracture length versus time.

In Fig. 24a and b, the numerical and experimental responses are compared in terms of the load–displacement plot and the fracture length versus time plot, for two opening displacement velocities.

As can be seen from the above results, the comparison between simulation and experiments is satisfactory and confirms the potentiality of the proposed models.

A further discussion on experimental evidences concerning time-dependent delamination and on the use of interface model of the kind proposed in Section 2 can be found in Corigliano et al. (1997a,b, 1998).

7. Closing remarks

In this paper, two time-dependent interface models have been proposed. The first one is viscoplastic with the following main characteristics: irreversible viscoplastic displacement discontinuities; evolution law of the Perzyna kind, unilateral effect in the direction normal to the interface; softening behaviour in order to simulate interface degradation.

The second interface model proposed is time-dependent elastic-damage, its main characteristics are as follows: anisotropic model with three damage variables, unilateral effect in the direction normal to the interface; evolution law of damage variables governed by a potential function.

The two models proposed have been discussed in details, and the analytical responses in pure mode (mode I, II or III) under monotonic loading conditions of both models have been derived for particular values of the model parameters. A time integration procedure of the Runge–Kutta kind has been applied for the two models for the solution of a single step in non-linear analyses. The formulation of a finite element non-linear analysis has also been discussed.

The potentialities of the proposed formulation have been shown through the finite element numerical simulation of interlaminar fracture specimens and the comparison between numerical and experimental results.

The results presented in the paper are part of a work in progress; issues, which are now being dealt with, are the following:

- Improved time step integration and interface element formulation in order to reduce computing time.
- Parameter identification of the interface models. This is a crucial point whenever complicate non-linear constitutive models and in particular interface models are considered.
- Extensive experimentation, in order to put in evidence when the delamination phenomenon is truly time dependent.
- Study of interaction among different causes of rate dependence and non-linearity: viscosity of layers and/or of the process zone, damage processes in the layers, etc.

Acknowledgements

Fruitful discussion with prof. R. Frassine and his permission to publish some experimental results are gratefully acknowledged. This paper has been carried out in the framework of the project PF MSTA II contract no. 97.00906.PF34, financed by CNR (Italian National Research Council).

Appendix A. Derivation of Eqs. (22) and (23)

The equations governing the non-linear phase for the viscoplastic interface model are given in Eq. (21) and re-written here:

$$\mathbf{t}_{n+1} = \mathbf{K}\left([\mathbf{u}]_{n+1} - [\mathbf{u}]^{\mathrm{vp}}_{n+1}\right), \tag{A.1}$$

$$[\mathbf{u}]^{\mathrm{vp}}_{n+1} = [\mathbf{u}]^{\mathrm{vp}}_{n} + \Delta\tau\left((1-\vartheta)[\dot{\mathbf{u}}]^{\mathrm{vp}}_{n} + \vartheta[\dot{\mathbf{u}}]^{\mathrm{vp}}_{n+1}\right), \tag{A.2}$$

$$\lambda_{n+1} = \lambda_n + \Delta\tau\left((1-\vartheta)\dot{\lambda}_n + \vartheta\dot{\lambda}_{n+1}\right), \quad \vartheta \in [0,1], \tag{A.3}$$

$$[\dot{\mathbf{u}}]^{\mathrm{vp}}_{n+1} = [\dot{\mathbf{u}}]^{\mathrm{vp}}_{n} + \left(\left.\frac{\partial[\dot{\mathbf{u}}]^{\mathrm{vp}}}{\partial\mathbf{t}}\right|_n\right)^{\mathrm{T}}\Delta\mathbf{t} + \left(\left.\frac{\partial[\dot{\mathbf{u}}]^{\mathrm{vp}}}{\partial\lambda}\right|_n\right)^{\mathrm{T}}\Delta\lambda, \tag{A.4}$$

$$\dot{\lambda}_{n+1} = \dot{\lambda}_n + \left(\left.\frac{\partial\dot{\lambda}}{\partial[\dot{\mathbf{u}}]^{\mathrm{vp}}}\right|_n\right)^{\mathrm{T}}\Delta[\dot{\mathbf{u}}]^{\mathrm{vp}}, \tag{A.5}$$

$$[\dot{\mathbf{u}}]^{\mathrm{vp}} = \gamma f^N(\mathbf{t},\lambda)\frac{\partial f}{\partial\mathbf{t}}, \quad \dot{\lambda} = \sqrt{[\dot{\mathbf{u}}]^{\mathrm{vp}^{\mathrm{T}}}[\dot{\mathbf{u}}]^{\mathrm{vp}}}. \tag{A.6}$$

By combining relations (A.3) and (A.5), it is possible to obtain an expression for the increment $\Delta\lambda$, which can be substituted in (A.4) in order to obtain

$$\left(I - \Delta\tau\vartheta\left(\left.\frac{\partial[\dot{\mathbf{u}}]^{\mathrm{vp}}}{\partial\lambda}\right|_n\right)^{\mathrm{T}}\left(\left.\frac{\partial\dot{\lambda}}{\partial[\dot{\mathbf{u}}]^{\mathrm{vp}}}\right|_n\right)^{\mathrm{T}}\right)\Delta[\dot{\mathbf{u}}]^{\mathrm{vp}} = \left(\left.\frac{\partial[\dot{\mathbf{u}}]^{\mathrm{vp}}}{\partial\mathbf{t}}\right|_n\right)^{\mathrm{T}}\Delta\mathbf{t} + \Delta\tau\left(\left.\frac{\partial[\dot{\mathbf{u}}]^{\mathrm{vp}}}{\partial\lambda}\right|_n\right)^{\mathrm{T}}\dot{\lambda}_n. \tag{A.7}$$

From the definition (A.6b) of $\dot{\lambda}$, it results that

$$\left(\left.\frac{\partial\dot{\lambda}}{\partial[\dot{\mathbf{u}}]^{\mathrm{vp}}}\right|_n\right)^{\mathrm{T}} = \frac{\left([\dot{\mathbf{u}}]_n^{\mathrm{vp}}\right)^{\mathrm{T}}}{\dot{\lambda}_n}. \tag{A.8}$$

By defining

$$\mathbf{A} \equiv \left(I - \Delta\tau\vartheta\mathbf{C}\frac{\left([\dot{\mathbf{u}}]_n^{\mathrm{vp}}\right)^{\mathrm{T}}}{\dot{\lambda}_n}\right)^{-1}, \quad \mathbf{B} \equiv \left(\left.\frac{\partial[\dot{\mathbf{u}}]^{\mathrm{vp}}}{\partial\mathbf{t}}\right|_n\right)^{\mathrm{T}}, \quad \mathbf{C} \equiv \left(\left.\frac{\partial[\dot{\mathbf{u}}]^{\mathrm{vp}}}{\partial\lambda}\right|_n\right)^{\mathrm{T}}. \tag{A.9}$$

From Eq. (A.7), one obtains

$$\Delta[\dot{\mathbf{u}}]^{\mathrm{vp}} = \mathbf{AB}\Delta\mathbf{t} + \Delta\tau\mathbf{AC}\dot{\lambda}_n. \tag{A.10}$$

Now, combining Eqs (A.10), (A.2) and (A.1), the following expression for the increment of traction in the step is arrived at:

$$\mathbf{t}_{n+1} = \mathbf{t}_n + \mathbf{K}_n^*\Delta[\mathbf{u}] - \Delta\mathbf{q}_n, \tag{A.11}$$

where

$$\mathbf{K}_n^* \equiv (\mathbf{I} + \Delta\tau\vartheta\mathbf{KAB})^{-1}\mathbf{K}, \qquad \Delta\mathbf{q}_n \equiv \Delta\tau\mathbf{K}_n^*\left([\dot{\mathbf{u}}]_n^{\mathrm{vp}} + \Delta\tau\vartheta\mathbf{AC}\dot{\lambda}_n\right). \tag{A.12}$$

Matrices **B** and **C** can be obtained by computing the derivatives of function f (Eq. (4)) and introducing them in the expressions below:

$$\mathbf{B} = \gamma N f(\mathbf{t},\lambda)^{N-1}\begin{bmatrix} \left(\frac{\partial f}{\partial t_1}\right)^2 & \left(\frac{\partial f}{\partial t_1}\right)\left(\frac{\partial f}{\partial t_2}\right) & \left(\frac{\partial f}{\partial t_1}\right)\left(\frac{\partial f}{\partial t_3}\right) \\ & \left(\frac{\partial f}{\partial t_2}\right)^2 & \left(\frac{\partial f}{\partial t_3}\right)\left(\frac{\partial f}{\partial t_2}\right) \\ \text{sym} & & \left(\frac{\partial f}{\partial t_3}\right)^2 \end{bmatrix} + \gamma f(\mathbf{t},\lambda)^N \begin{bmatrix} \frac{\partial^2 f}{\partial t_1^2} & \frac{\partial^2 f}{\partial t_1\partial t_2} & \frac{\partial^2 f}{\partial t_1\partial t_3} \\ & \frac{\partial^2 f}{\partial t_2^2} & \frac{\partial^2 f}{\partial t_2\partial t_3} \\ \text{sym} & & \frac{\partial^2 f}{\partial t_3^2} \end{bmatrix}, \tag{A.13}$$

$$\mathbf{C}^{\mathrm{T}} = \gamma N(f(\mathbf{t},\lambda))^{N-1}h\begin{bmatrix} \frac{\partial f}{\partial t_1} & \frac{\partial f}{\partial t_2} & \frac{\partial f}{\partial t_3} \end{bmatrix}. \tag{A.14}$$

Appendix B. Derivation of Eqs. (26)–(28)

The equations governing the non-linear phase for the elastic-damage interface model are given in Eq. (25) and re-written here:

$$\mathbf{t}_{n+1} = (\mathbf{I} - \mathbf{D}_{n+1})\mathbf{K}[\mathbf{u}]_{n+1}, \quad \mathbf{D} \equiv \mathrm{diag}(D_i), \ \ \mathbf{K} \equiv \mathrm{diag}(K_i), \ \ i = 1,2,3, \tag{B.1}$$

$$\mathbf{D}_{n+1} = \mathbf{D}_n + \Delta\tau((1-\vartheta)\dot{\mathbf{D}}_n + \vartheta\dot{\mathbf{D}}_{n+1}), \tag{B.2}$$

$$\lambda_{n+1} = \lambda_n + \Delta\tau((1-\vartheta)\dot{\lambda}_n + \vartheta\dot{\lambda}_{n+1}), \quad \vartheta \in [0,1], \tag{B.3}$$

$$\dot{\mathbf{D}}_{n+1} = \dot{\mathbf{D}}_n + \left(\left.\frac{\partial\dot{\mathbf{D}}}{\partial\mathbf{Y}}\right|_n\right)^{\mathrm{T}}\Delta\mathbf{Y} + \left(\left.\frac{\partial\dot{\mathbf{D}}}{\partial\lambda}\right|_n\right)^{\mathrm{T}}\Delta\lambda, \tag{B.4}$$

$$\dot{\lambda}_{n+1} = \dot{\lambda}_n + \left(\frac{\partial \dot{\lambda}}{\partial \dot{\mathbf{D}}} \bigg|_n \right)^{\mathrm{T}} \Delta \dot{\mathbf{D}}, \tag{B.5}$$

$$\dot{D}_i = \hat{\gamma}_i \hat{f}(\mathbf{Y}, \lambda)^N, \quad i = 1, 2, 3, \quad \dot{\lambda} = \sqrt{\sum_{i=1}^{3} \dot{D}_i^2}. \tag{B.6a, b}$$

By combining relations (B.3) and (B.5), it is possible to obtain an expression for the increment $\Delta\lambda$ which can be substituted in (B.4) in order to obtain

$$\left(I - \Delta\tau\vartheta \left(\frac{\partial \dot{\mathbf{D}}}{\partial \lambda} \bigg|_n \right)^{\mathrm{T}} \left(\frac{\partial \dot{\lambda}}{\partial \dot{\mathbf{D}}} \bigg|_n \right)^{\mathrm{T}} \right) \Delta \dot{\mathbf{D}} = \left(\frac{\partial \dot{\mathbf{D}}}{\partial \mathbf{Y}} \bigg|_n \right)^{\mathrm{T}} \Delta \mathbf{Y} + \Delta\tau \left(\frac{\partial \dot{\mathbf{D}}}{\partial \lambda} \bigg|_n \right)^{\mathrm{T}} \dot{\lambda}_n. \tag{B.7}$$

From the definition (B.6a,b) of $\dot{\lambda}$, it results that

$$\left(\frac{\partial \dot{\lambda}}{\partial \dot{\mathbf{D}}} \bigg|_n \right)^{\mathrm{T}} = \frac{\dot{\mathbf{D}}_n^{\mathrm{T}}}{\dot{\lambda}_n}. \tag{B.8}$$

By defining

$$\hat{\mathbf{A}} \equiv \left(I - \Delta\tau\vartheta \hat{\mathbf{C}} \frac{\dot{\mathbf{D}}_n^{\mathrm{T}}}{\dot{\lambda}_n} \right)^{-1}, \quad \hat{\mathbf{B}} \equiv \left(\frac{\partial \dot{\mathbf{D}}}{\partial \mathbf{Y}} \bigg|_n \right)^{\mathrm{T}}, \quad \hat{\mathbf{C}} \equiv \left(\frac{\partial \dot{\mathbf{D}}}{\partial \lambda} \bigg|_n \right)^{\mathrm{T}}. \tag{B.9}$$

From Eq. (B.7), one obtains

$$\Delta \dot{\mathbf{D}} = \hat{\mathbf{A}} \hat{\mathbf{B}} \Delta \mathbf{Y} + \Delta\tau \hat{\mathbf{A}} \hat{\mathbf{C}} \dot{\lambda}_n. \tag{B.10}$$

Now, combining Eqs. (B.10) and (B.2) and (B.1), the following expression for the increment of traction in the step is arrived at:

$$\mathbf{t}_{n+1} = (\mathbf{I} - \mathbf{D}_{n+1}) \mathbf{K} [\mathbf{u}]_{n+1}, \tag{B.11a}$$

$$\mathbf{D}_{n+1} = \mathbf{D}_n + \Delta\tau \left(\dot{\mathbf{D}}_n + \vartheta \hat{\mathbf{A}} \hat{\mathbf{B}} \Delta \mathbf{Y} + \vartheta \Delta\tau \hat{\mathbf{A}} \hat{\mathbf{C}} \dot{\lambda}_n \right). \tag{B.11b}$$

Matrices $\hat{\mathbf{B}}$ and $\hat{\mathbf{C}}$ can be obtained by computing the derivatives of function $\hat{f}$ (Eq. (9)) and introducing them in the expressions below:

$$\hat{\mathbf{B}} = N \hat{f}(\mathbf{Y}, \lambda)^{N-1} \begin{bmatrix} \hat{\gamma}_1 \left(\frac{\partial \hat{f}}{\partial Y_1} \right) & \hat{\gamma}_1 \left(\frac{\partial \hat{f}}{\partial Y_2} \right) & \hat{\gamma}_1 \left(\frac{\partial \hat{f}}{\partial Y_3} \right) \\ \hat{\gamma}_2 \left(\frac{\partial \hat{f}}{\partial Y_1} \right) & \hat{\gamma}_2 \left(\frac{\partial \hat{f}}{\partial Y_2} \right) & \hat{\gamma}_2 \left(\frac{\partial \hat{f}}{\partial Y_3} \right) \\ \hat{\gamma}_3 \left(\frac{\partial \hat{f}}{\partial Y_1} \right) & \hat{\gamma}_3 \left(\frac{\partial \hat{f}}{\partial Y_2} \right) & \hat{\gamma}_3 \left(\frac{\partial \hat{f}}{\partial Y_3} \right) \end{bmatrix}, \tag{B.12}$$

$$\mathbf{C}^{\mathrm{T}} = N (\hat{f}(\mathbf{Y}, \lambda))^{N-1} \hat{h} \begin{bmatrix} \hat{\gamma}_1 & \hat{\gamma}_2 & \hat{\gamma}_3 \end{bmatrix}. \tag{B.13}$$

The tangent matrix can be obtained starting from Eq. (B.11); it results that

$$\mathbf{K}_{\mathrm{T}} \equiv \left(\frac{\partial \mathbf{t}_{n+1}}{\partial [\mathbf{u}]_{n+1}} \right)^{\mathrm{T}} = \left((\mathbf{I} - \mathbf{D}_{n+1}) \mathbf{K} - \Delta\tau\vartheta \left(\frac{\partial \mathbf{Y}_{n+1}}{\partial [\mathbf{u}]_{n+1}} \right)^{\mathrm{T}} \hat{\mathbf{A}} \hat{\mathbf{B}} \left(\frac{\partial \mathbf{Y}_{n+1}}{\partial [\mathbf{u}]_{n+1}} \right) \right), \tag{B.14}$$

where the matrix $\left(\partial \mathbf{Y}_{n+1}/\partial[\mathbf{u}]_{n+1}\right)$ has the simple expression

$$\frac{\partial \mathbf{Y}_{n+1}}{\partial[\mathbf{u}]_{n+1}} = \operatorname{diag}\left[K_i[u]_i\right], \quad i = 1,2,3. \tag{B.15}$$

References

Aliyu, A.A., Daniel, I.M., 1985. Effects of strain rate on delamination fracture toughness of graphite/epoxy. Delamination and debonding of materials. In: Johnson W.S. (Ed.), American Society for Testing and Materials, ASTM STP 876. Philadelphia, pp. 336–348.

Allix, O., Ladevéze, P., 1992. Interlaminar interface modelling for the prediction of delamination. Int. J. Compos. Struct. 22, 235–242.

Allix, O., Ladevéze, P., Corigliano, A., 1995. Damage analysis of interlaminar fracture specimens. Compos. Struct. 31, 61–74.

Allix, O., Corigliano, A., 1996. Modeling and simulation of crack propagation in mixed-modes interlaminar fracture specimens. Int. J. Fract. 77, 111–140.

Bažant, Z.P., Beissel, S., 1994. Smeared-tip superposition method for cohesive fracture with rate effect and creep. Int. J. Fract. 65, 277–290.

Bolzon, G., Corigliano, A., 1997. A discrete formulation for elastic solids with damaging interfaces. Comp. Meth. Appl. Mech. Engng 140, 329–359.

Bradley, W.L., 1989. Relationship of matrix toughness to interlaminar fracture toughness. In: Friedrich, K. (Ed.), Application of Fracture Mechanics to Composite Materials. pp. 159–187.

Corigliano, A., 1993. Formulation, identification and use of interface models in the numerical analysis of composite delamination. Int. J. Solids Struct. 30, 2779–2811.

Corigliano, A., Ricci, M., Contro, R., 1997a. Rate dependent delamination in polymer-matrix composites. In: Owen, D.R.J., Oñate, E., Hinton, E. (Eds.), Proceedings of the Fifth International Conference on Computational Plasticity. Barcelona, CIMNE Barcelona, pp. 1168–1175.

Corigliano, A., Frassine, R., Ricci, M., 1997b. Rate-dependent interface models for the analysis of delamination in polymer-matrix composites. In: Rossmanith, H.P. (Ed.), Proceedings of DFI-1. Vienna, Balkema, Rotterdam, pp. 139–146.

Corigliano, A., Frassine, R., Ricci, M., 1998. Rate dependent fracture properties in the delamination of polymer-matrix composites. In: Oñate, E., Idelsohn, S.R. (Eds.), Proceedings of IV WCCM. Buenos Aires, CIMNE Barcelona.

Corigliano, A., Mariani, S., 1999. Parameter identification of interface models for the simulation of debounding in composites. In: N. Winldertich, Ed., Eccn 99, European Conf. Comp.

Crisfield, M.A., Mi, Y., Davies, G.A.O., Hellweg, H.B., 1997. Finite element methods and the progressive failure-modelling of composites structures. In: Owen, D.R.J., Onate, E., Hinton, E. (Eds.), Proceedings of the Fifth International Conference on Computational Plasticity. Barcelona, CIMNE Barcelona, pp. 239–254.

Davies, P., 1992. Interlaminar Fracture Testing of Composites. Mode I (DCB) Testing Protocol for ESIS-TC4.

Ferry, J.D., 1980. Viscoelastic Properties of Polymers, third ed. Wiley, New York.

Frassine, R., Rink, M., Pavan, A., 1993. Viscoelastic effects on intralaminar fracture toughness of epoxy/carbon fibre. Int. J. Comp. Mat. 27, 921–933.

Frassine, R., Pavan, A., 1995. Viscoelastic effects on the interlaminar fracture behaviour of thermoplastic matrix composites: I. Rate and temperature dependence in unidirectional PEI/carbon-fibre laminates. J. Comp. Sci. Tech. 54, 193–200.

Frassine, R., Rink, M., Pavan, A., 1996. Viscoelastic effects on the interlaminar fracture behaviour of thermoplastic matrix composites: II. Rate and temperature dependence in unidirectional PEEK/carbon-fibre laminates. Compos. Sci. Technol. 56, 1253–1260.

Friedrich, K., Walter, R., Carlsson, L.A., Smiley, A.J., Gillespie Jr., J.W., 1989. Mechanisms of rate effects on interlaminar fracture toughness of carbon/epoxy. J. Mat. Sci. 24, 3387.

Garg, A.C., 1988. Delamination – a damage mode in composite structures. Engng. Fract. Mech. 29, 557–584.

Hashemi, S., Kinloch, A.J., Williams, J.G., 1990. The effects of geometry, rate and temperature on the Mode I, Mode II and Mixed Mode I/II interlaminar fracture of carbon fibre/poly(ether–ether ketone) composites. J. Compos. Mat. 24, 918–956.

Jensen, H.M., Hutchinson, J.W., Kim, K.S., 1990. Decohesion of a cut prestressed film on a substrate. Int. J. Solids Struct. 26, 1099–1114.

Netmes, J.A., Spéciel, E., 1996. Use of a rate-dependent continuum damage model to describe strain-softening in laminated composites. Comp. Struct. 58 (6), 1083–1092.

Pandolfi, A., Krysl, P., Ortiz, M., 1999. Finite element simulation of ring expansion and fragmentation: the capturing of length and time scales through coherine models of fracture. Int. J. Fract 95, 1–18.

Perzyna, P., 1966. Fundamentals problems in visco-plasticity. Recent Advances in Appl. Mech., Academic Press, New York.

Popelar, C.H., Kanninen, M.F., 1980. A dynamic viscoelastic analysis of crack propagation and crack arrest in a double cantilever beam testing specimen. In: Hahan, G.T., Kanninen, M.F. (Eds.), Crack Arrest Methodology and Applications. American Society for Testing and Materials, ASTM STP 711, Philadelphia, pp. 5–23.

Satmani Naresh, C., Desai Chandra, S., Vulliet, L., 1996. An interface model to describe viscoplastic behavior. Int. J. Numer. Anal. Meth. Geomech. 20, 231–252.

Schellekens, J.C.J., De Borst, R., 1993. A non-linear finite element approach for the analysis of mode-I free edge delamination in composites. Int. J. Solids Struct. 30 (9), 1239–1253.

Smiley, A.J., Pipes, R.B., 1987. Rate effects on mode I interlaminar fracture toughness in composite materials. J. Compos. Mat. 21, 670–687.